Microstructure-based FE Modeling and Measurements of Magnetic Properties of Polymer Matrix-Metal Composites

Weizhen Sun

Thesis submitted to the faculty of the Virginia Polytechnic Institute and State University in partial fulfillment of the requirements for the degree of

Master of Science
In
Electrical Engineering

Guo-Quan Lu, Chair
Khai D. T. Ngo
Qiang Li

December 5th, 2016
Blacksburg, VA

Keywords: Modeling, Composite, Magnetic material

Microstructure-based FE Modeling and Measurements of Magnetic Properties of Polymer Matrix-Metal Composites

Weizhen Sun

Abstract

An increasing need for smaller, higher-power-density devices is driving the development of more advanced topologies for use in power architectures. The challenge, however, is to reduce the size of the passive components in circuit boards (e.g., the inductors), which are typically the most bulky. There are two ways to approach this problem. The first is to redesign the flux in the inductor in order to minimize its size; the second is to optimize the magnetic properties of the constituent magnetic materials, which include permeability, density, resistivity, core loss density, saturation magnetization value, fluidity, sintering temperature, and others. Compared to altering the nature of solid magnetic materials to reduce space constraints, modifying the magnetic composite is preferred.

The most popular candidates for use in magnetic composites are magnetic powders and polymer composites. In particular, when metal alloys are chosen as magnetic powders they have high initial permeability, high saturation magnetization values, but low electrical resistivity. Since polymers can serve as insulation materials, mixing metal alloys with polymers will increase electrical resistivity. The most common metal alloy used is nickel-iron (permalloy) and Metglas.

Since existing modeling methods are limited in (a) that multiphasic composites cannot be utilized and (b) the volume fraction of magnetic particles must be low, this investigation was

designed to utilize FE (finite element) simulation to analyze how magnetic properties change with the distribution of permalloy powder or Metglas flakes in composites. The primary magnetic properties of interest in this study are permeability and core loss density. Furthermore two kinds of magnetic composites were utilized in this investigation: a benzocyclobutene (BCB) matrix–permalloy and a benzocyclobutene (BCB) matrix-permalloy-based amorphous alloy (Metglas 2705M) material.

In our FE simulations, a BCB matrix–permalloy composite was utilized in a body-centered cubic model with half-diameter smaller particles serving as padding. The composite was placed in a uniform magnetic field surrounded by a material whose relative permeability was equal to zero in simulation. In comparison to experimental results, our model was able to predict permeability of composites with volume fraction higher than 52%. It must be noted, however, that although our model was able to predict permeability with only 10% off, it was less effective with respect to core loss density findings. The FE model also showed that permeability will increase with an increasing volume fraction of magnetic particles in the composite. To modify the properties of the composite material, the model of the BCB matrix-permalloy-Metglas composite followed model simulations up to the point at which flakes were inserted in BCB matrix-permalloy composite. The thickness of flakes was found to be an important factor in influencing resulting magnetic properties. Specifically, when the thickness of flakes decreased to quarter size at the same volume fraction, the permeability increased by 15%, while core loss density decreased to a quarter of the original value. The analysis described herein of the important relationship between magnetic properties and the composites is expected to aid in the development and design of new magnetic composite materials.

Microstructure-based FE Modeling and Measurements of Magnetic Properties of Polymer Matrix-Metal Composites

Weizhen Sun

General Audience Abstract

Power converters are essential for a wide variety of electronic applications (e.g., mobile phones, motor drives, etc.). And with the current push toward miniaturization, power converters that are smaller in size and feature higher power density are demanded. The most challenging aspect of reducing overall size while maintaining or, preferably, increasing the power density of a power converter is to reduce the size of the passive components in the circuit boards (e.g., the inductors). To optimize the performance of an inductor, the magnetic properties of the constituent magnetic materials in an inductor must be well designed. In particular, scientists and engineers are focusing on the two most important characteristics of a magnetic material—namely its permeability and core loss density.

In order to achieve the objective of high relative permeability and low core loss density, the incorporation of magnetic powders and polymer composites into the fabrication of magnetic materials is being considered. Since this method tends to require a great deal of trial and error to determine optimal fabrication parameters, it can be both time consuming and costly. This study, therefore, was designed to simplify the fabrication process by investigating the effects of altering

the parameters of a number of constituent components in a series of composites. Specifically, this investigation targeted the impact of altering the volume percentage, the shape, and the species of each component on the properties of composite materials by simulation, which was useful in predicting the performance of the magnetic materials under scrutiny. The simulation method utilized herein was FE (finite element), which was effective in determining the permeability and core loss density of the magnetic properties of interest in this study.

Acknowledgement

I own my deepest gratitude to my adviser, Dr. Guo-Quan Lu, for his knowledge and patience. I credit him with leading me to the field of power electronics, and without his guidance I would not have been able to complete this work. I deeply appreciate his patience with every aspect of my research. Furthermore, he not only taught me essential technical and analytical methods, but he also assisted me with communication and presentation skills as well.

I would also like to express my appreciation to Dr. Khai D. T. Ngo, whose guidance on technical issues was invaluable. His creative ideas and experience helped me overcome multiple roadblocks along this journey. I am grateful for his kindness and his advice..

Furthermore, I am very grateful to Dr. Qiang Li for accepting my invitation to serve on my committee.

I want to thank Dr. Christine B. Burgoyne and Mr. Laurie Good. They helped with writing and provided guidance on the thesis development.

Moreover, I would like to thank Yi Yan, Ting Ge, and Han Cui. They always encouraged me and gave me helpful suggestions when I encountered any difficulties. Thank you all for sharing your knowledge with me.

In addition, I extend my thanks to all the professors, staff, and students in CPES and in my immediate research group—together you provided a wonderful academic environment whereby we were able to exchange ideas. Thank you all for the unselfish help you provided.

Furthermore, my thanks go to the National Science Foundation (NSF) for the generous support on the project. Without NSF support, I would not have been able to contribute to such an interesting project.

Finally, but most importantly, I would like to thank my parents, Mr. Qifeng Sun and Mrs. Xuewen Yu. Your love supported me during every minute of the two years it took to complete this Master's degree. Your encouragement gave me the strength to move forward no matter what challenge I was facing.

Table of Contents

List of Figures

List of Tables

Chapter 1. Introduction

1.1 Application of magnetic materials in power electronics

The use of magnetic materials in power electronics continues to grow in importance. In power converters, for example, transformers and inductors play essential roles. Consider the example of a buck converter (also known as a step-down converter), which features a functional circuit to step down DC voltage to a lower voltage at high frequency. As illustrated in Fig. 1, there are two switches in the converter producing rectangular periodic waveforms. When V is equal to V_g, the energy is retained in the inductor; when V is equal to zero, the inductor performs as a battery, providing the energy to the load [1].

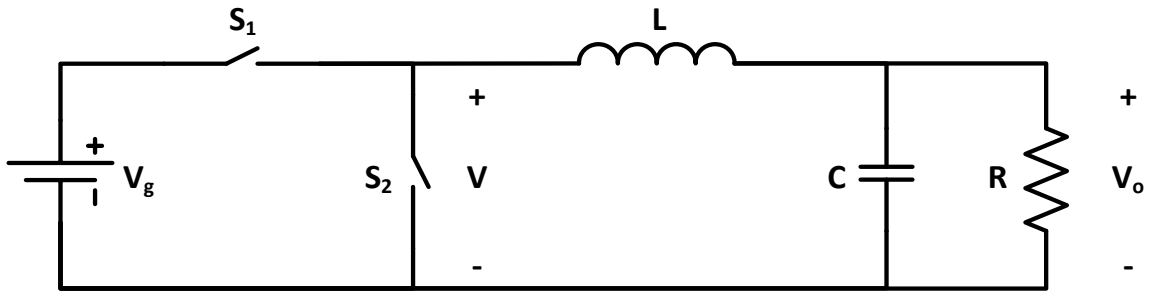

Fig. 1. Conventional buck converter topology with ideal switches.

Nowadays, the evolution of power architectures is largely driven by the need for higher efficiencies, higher power densities, and smaller sizes. The growing industrial importance of these factors has spurred the development of a variety of converters. The power density of some point of load (POL) converters is shown in Fig. 2 [2].

.

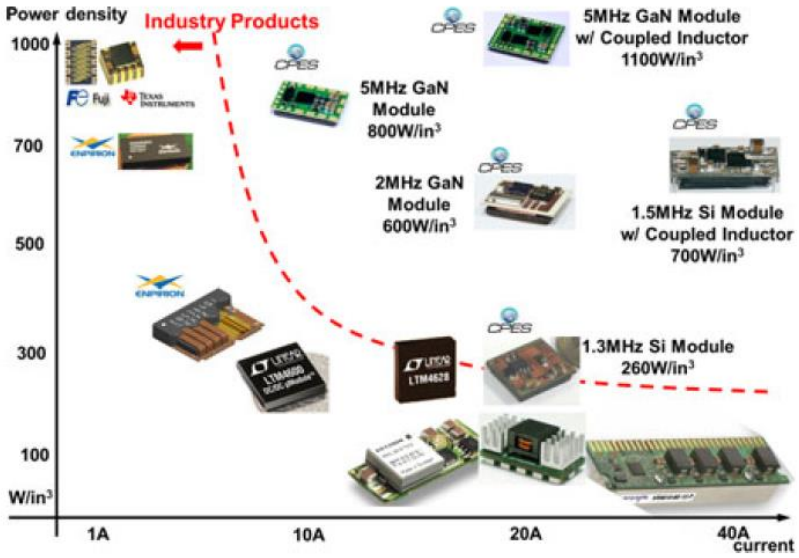

Fig. 2. Power density of some typical converters [2].

Note, however, that the passive components in these circuit structures—principally the inductors and capacitors—tend to be quite bulky. In order to decrease total volume of the circuit board, it is important to shrink the size of the inductors.

1.1.1 Overview of integration of magnetic components

There are two ways to meet the demand for high-efficiency and high-power-density power converters: one is by increasing switching frequency, and the other is by integrating magnetic composites. Due to the fact that increasing switching frequency helps to reduce the size and weight of the board, which is increasingly desirable for a range of industrial applications, tremendous R&D efforts are targeting the area of switches—from silicon semiconductors to gallium nitride (GaN) semiconductors [3].

As shown in Fig. 3, there are numerous methods for integrating magnetic components at various output currents and frequencies. In general, however, the methods can be classified into three categories: wafer-level, package-level, and board-level integration [4].

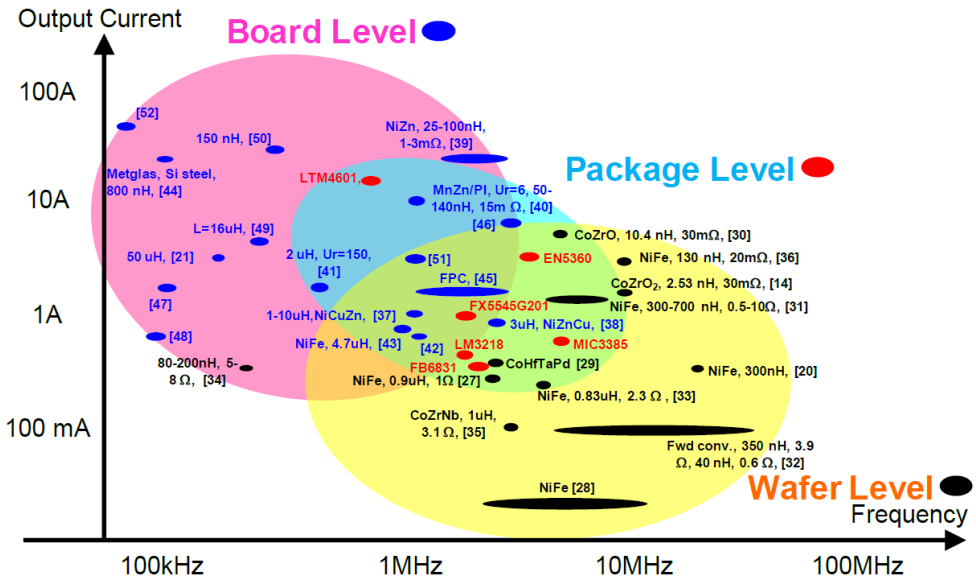

Fig. 3. Magnetic integration methods at various output currents and frequencies [4].

Package-level and board-level integration are commonly used in industry and therefore the mostly widely represented of the methods in the academic literature. There are three types of geometries designed to facilitate the integration of inductors at the package-level and board-level: solenoid, meander-type, and spiral [5]. Fig. 4 provides examples of the three geometries.

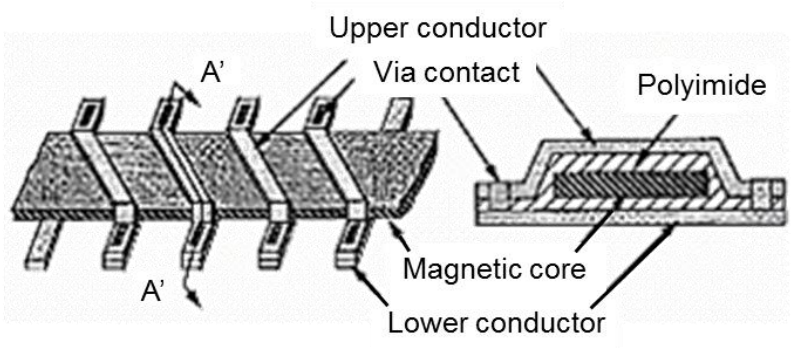

(a)

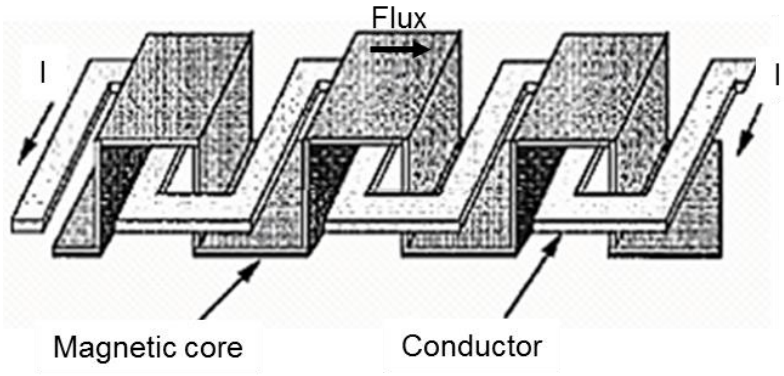

(b)

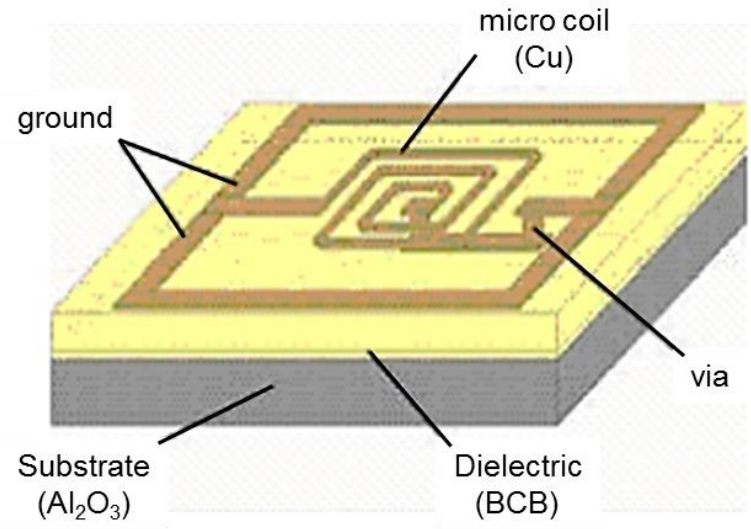

(c)

Fig. 4. Three geometries to realize the integration of an inductor: (a) integrated inductor in a solenoid structure [6]; (b) integrated inductor in a meander-type structure [7]; and (c) integrated inductor in a spiral structure [8].

1.1.2 Challenges of integration

As already noted, in order to integrate the functional parts of a converter into a small effective package, researchers have labored to overcome significant roadblocks in reducing the overall volume of the passive components [5, 9, 10]. For example, while increasing frequency can reduce the size of the module by decreasing the inductance and capacitance requests of the circuit, this approach has the unwanted side effects of increasing the impact of circuit parasitic parameters and amplifying magnetic loss as frequencies increase. In order to address the first issue and decrease parasitic parameters, it is essential to design a structure that minimizes the number of winding of inductor [11]. In addition to modifying the structure of both the transformer and the inductor, the component materials must also be considered.

The magnetic loss P_v includes classical eddy current loss P_c, static hysteresis loss P_h, and excess loss P_e. Thus, magnetic loss can be computed according to the following equation:

$$P_v = P_h + P_c + P_e = k_h f B_m^{\beta} + k_c (f B_m^{\beta})^2 + k_e (f B_m^{\beta})^{1.5} \quad (1)$$

where the coefficients k_h, k_c, k_e are given for certain material, as well as the parameter β. Based on this equation, the total magnetic loss per unit volume P_v is in terms of frequency f. It is clear, then, that when switching frequency increases, magnetic loss will also increase rapidly.

Another barrier to integrating a converter into a smaller component has to do with the issue of thermal management. As the packaging become smaller, surface areas that contribute to overall cooling are also minimized—thereby causing the whole circuit to heat up. At the same time, increasing switching frequency generates higher switching loss. As a result, there is a thermal

problem that must be addressed—for instance, chips break down and the solder is at risk for melting [12].

1.2 Review of microstructure-based modeling

To improve the efficiencies and power densities of power circuits, a magnetic material with high permeability and low core loss density is required. Additionally, a lower sintering temperature to simplify fabrication is also essential. Currently, the most common soft magnetic materials include ferrites and powder cores. Soft ferrites, which feature an expansive range of permeability and low core loss density values, are widely applied in power electronics. However, the high sintering temperature needed to utilize ferrites represents a significant roadblock. To achieve low temperature fabrication, researchers have been investigating the use of powder cores, which are fabricated from magnetic powders and an insolation layer. Specifically, the magnetic powders provide permeability, while the insolation layer decreases the electrical resistivity of the composite material.

A great deal of research in this area has been targeted at optimizing the magnetic properties of composite materials, determining the most effective constituent components. Like so much of basic research, a great deal of what we know about soft magnetic composite materials has been achieved via trial and error [13, 14]. More recently, researchers have been developing analytical models to predict the properties of magnetic material, thereby providing guidance to the fabrication of composite materials [15]. One particular principle stands out in this regard: effective medium theory (EMT).

The most popular way to model composites for use in magnetic materials is through the use of effective medium theory. It is well known that experimental systems tend to be disorderly and unsystematic. In order to build a more reliable experimental system for use in this area, EMT is utilized when the field wavelength is much larger than the particle size—for instance, when the wavelength of a 1 MHz electromagnetic field is 300m and the particle size is always at the micrometer level [16].

One of the more common formulas for representing electromagnetic properties is the Maxwell-Garnett (MG) model, which is a formula for modeling the relative permittivity and permeability of binary mixtures. This formulation was derived from experiment measurements. Using permittivity derivation as an example, the filler is randomly distributed in the host of the composite (as shown in Fig. 5). The formulation is then derived from the permittivity of the composite in measured experiment (as shown in Fig. 6) [16].

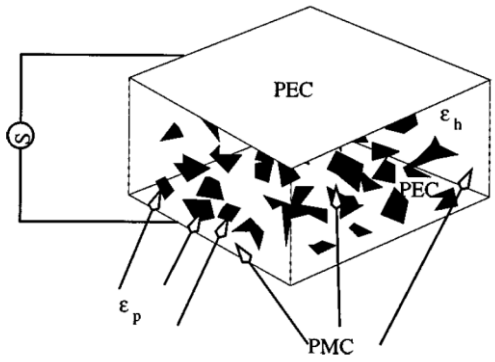

Fig. 5. Unit volume of a composite in an ideal capacitor to derive effective permittivity [16].

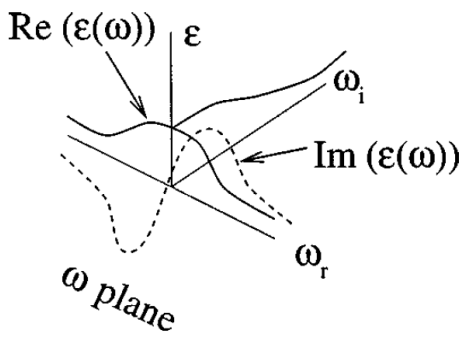

Fig. 6. Effective permittivity of the composite in the complex frequency plane [16].

The function of permeability is the same as permittivity in an MG formulation [17], which is:

$$\frac{\mu_r - 1}{1 + A_w(\mu_r - 1)} = \frac{v_A(\mu_{B_r} - 1)}{1 + A_w(\mu_{B_r} - 1)} \tag{2}$$

where μ_r is the relative permeability of the composite material; μ_{B_r} is the relative permeability of component B in the composite; v_A is the volume fraction of component A; and Aw is the shape factor of magnetic particles. The function of the shape factor has been researched for quite a long time, and is presented in the following equations [18]:

$$A_w = \frac{1}{2A_R} \tag{3}$$

$$A_R = \frac{S_n}{S_L} \tag{4}$$

where S_n is the area of a particle across the flux; and S_f is the area of the lateral surface of a particle.

Since the host in a given composite material is sometimes bianisotropic instead of biisotropic (which is assumed in the GM formulation), the Bruggeman model represents an improved formulation [19], as described in the following equation:

$$\frac{v_A(\mu_{B_r} - \mu_r)}{\mu_r + A_w(\mu_{B_r} - \mu_r)} = (1 - v_A)\frac{\mu_r - 1}{\mu_r - A_w(\mu_r - 1)} \tag{5}$$

This particular numerical model features a number of limitations that must be noted. First, both of the solutions can calculate permeability well at low volume fraction (less than 47 vol.%) [20]. However, when the volume fraction is higher, the deviation between calculation and experimental results is also higher. Indeed, for magnetic materials, the volume percent of magnetic particles is always higher than 50 vol.%. Second, the MG model works well for biphasic composites at high particle density with regime limitations, but it is limited in the case of multiphasic composites [21]. Third, this model is ineffective for describing the size distribution of particles in the composite [22]. Finally, since both of models rely on experimental measurements, the use of different materials would require recalculating the constant in the models.

Prior to conducting numerical modeling on composites using effective medium theory, early research pioneers established a relationship between the properties of composites and their constituent components by studying and modeling composite structures. The earliest such study occurred 1873, which resulted in the Maxwell equation for highly dilute composites [23]:

$$\frac{\mu}{\mu_B} = 1 + \frac{3v_A}{\frac{a+2}{a-1} - v_A} \tag{6}$$

where a is the ratio of permeability of two components in the composite material; $\mu = \mu_0\mu_r$ is the permeability of the composite material ($\mu_0 = 4\pi \times 10^{-7}$ H/m is a physical constant called vacuum permeability); and $\mu_B = \mu_0\mu_{B_r}$ is the permeability of the composite material. In this model, all the particles are spherical in shape and do not impact each other. To address variations in particle shape, Wiener developed his equation in 1974 [24, 25]:

$$\frac{\mu}{\mu_B} = 1 + \frac{(1 + A_w)v_A}{\frac{a + A_w}{a - 1} - v_A} \tag{7}$$

It must be noted, however, that this formula still features two limitations: very low volume percentage and the fact that particles cannot impact each other. To determine more about non-dilute dispersion, a simple cubic (s.c.) lattice was adopted as a unit cell to extend the Maxwell equation [25-27]:

$$\frac{\mu}{\mu_B} = 1 + 3v_A\left(\frac{a + 2}{a - 1} - v_A - \frac{k_1 v_A^{\frac{10}{3}}}{\frac{a + \frac{4}{3}}{a - 1} - k_2 v_A^{\frac{7}{3}}} - \frac{k_3(a - 1)v_A^{\frac{14}{3}}}{a + \frac{6}{5}}\right)^{-1} \tag{8}$$

Where k_1, k_2, and k_3 are constant. However, the maximum package of particle can only reach a level up to $v_A = \pi/6$ (50%) when all the particles are in contact with each other. Furthermore, it is impossible for spherical particles to encompass the entire space in a simple cubic lattice. In response, over 30 years ago Petropoulos studied the permeability of binary composite polymeric materials and reported that cubic particles can achieve $v_A = 1$. Still there is drawback to his approach in that the cubic shape is not as amenable as the spherical shape in describing particles

[28]. It must be noted that in addition to ideal lattice models, a number of numerical and analytical models featuring random particle distributions have been studied—for example, those whose particles are flake shaped [25]. However, they have only been applied to specific cases and cannot be easily applied to the current investigation.

1.3 Organization of the thesis

To meet the increasing demand for new and sophisticated power electronics, novel soft magnetic materials with high permeability, low loss at high frequency (up to MHz), low sintering temperature, and high saturation flux density are urgently needed. Currently, however, there are no bulk materials that can meet all these demands. Thus, a range of advanced composite materials is needed that can be incorporated in new magnetic devices [29]. Additionally, modeling studies are needed to determine the relationship between the physical and electromagnetic properties of composite materials, which will then guide materials researchers in fabricating new composites. This area of research is also limited by the fact that existing models cannot easily be applied to the design of novel magnetic composites.

Therefore, this study was design to investigate two models that can be applied to the development of advanced magnetic composite materials: (a) the model of biphasic composites, and (b) the model of multiphasic composites. The first chapter provides some scholarly background for this discussion and details the specific objectives of the current investigation. The second chapter discusses the structure of the microstructure model. The third chapter explains the modeling of polymer matrix-metal composites—and in particular introduces the first type of magnetic material composite of importance to this investigation—namely, a

polymer/magnetic powder composite. The fourth chapter discusses the effects of flakes in magnetic composites by describing the second important variety of magnetic composite materials: polymer/magnetic powder/magnetic flakes composites. The third and fourth chapters will provide guidance to the material fabrication. Finally, the fifth chapter will summarize the results of this investigation and suggest avenues for future research.

Chapter 2. Description of the structure of the FE model of composites

This chapter describes the creation of a model for developing magnetic composites. The accuracy of the model relies on determining the microstructure of the magnetic composite, which is achieved through the use of scanning electron microscopy (SEM). Once a sample is fabricated, a beam of electrons is passed through it, which then affords a detailed micrograph of the sample. From this micrograph, the properties of each composite—including constituent particle size and the gap between particles—can be determined. Based on the microstructure from the micrograph, a unit cell model can then be developed.

2.1 Structure of composite material

Composite soft magnetic materials are referred to as dialectical magnetic materials; typically, they feature relatively high permeability, low core loss density and good thermal performance at middle and high frequencies [21, 30, 31]. Because composite magnetic materials must feature low core loss density, they are typically fabricated with magnetic powder particles surrounded by a dielectric material. In general, these dielectric materials are isolate particles, which are useful for promoting the high frequency of these soft magnetic materials [32]. Additionally, since the dielectric host performs like an air gap, permeability decreases. Fig. 7 shows a conceptual micrograph of a magnetic composite with its characteristic spherical particles in a unit area, whose side length is L. The green background is the surrounding polymer isolates, and the blue particles are magnetic powder particles whose diameter is D.

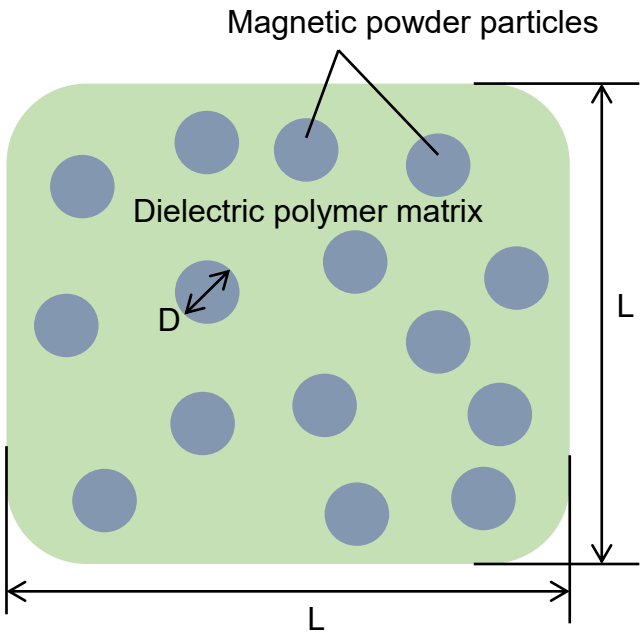

Fig. 7. Conceptual micrograph of a magnetic composite material.

2.2 FE model structure of polymer matrix-magnetic particle composites

Researchers have developed a number of theories and models to elucidate the relationship between a composite material's microstructure and its inherent physical properties. In particular, effective medium theory or EMT is useful for determining the average properties of a given composite material. Such components typically include the composite's essential magnetic properties such as permeability and core loss density. Other properties of interest for magnetic materials include the volume faction, particle shape, and permeability of each component in the composite, which can be described by their average number.

It must be noted, however, that numerical modeling is limited in that it is not useful for determining the properties of multiple scattered composites. Given this drawback, we adopted

the analytical model for this investigation. In order to represent a given composite material with limited volume using a theoretical model, a unit cell is proposed to describe the composite material. Moreover, the unit cell can describe the average value of properties of the composite material. Fig. 8 provides a 2D model of a typical magnetic composite material in a unit area [25, 33].

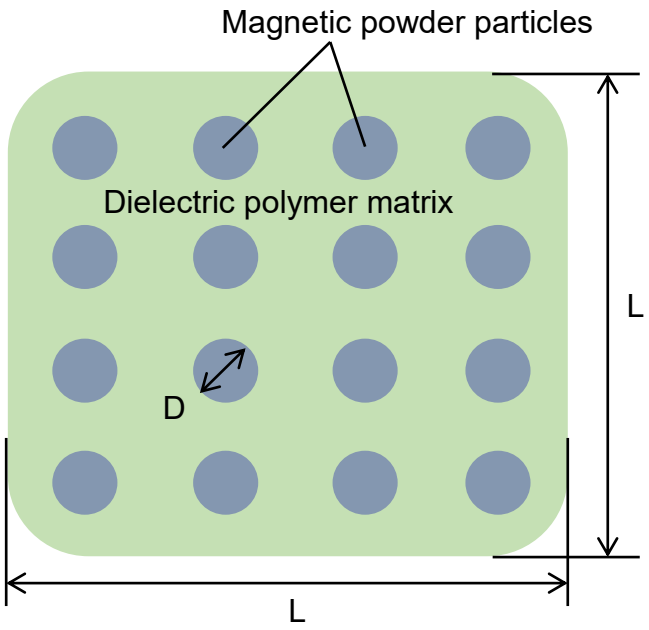

Fig. 8. 2D model of magnetic composite material.

As with any 2D model that attempts to represent a three-dimensional material, a number of limitations are present. For example, the particle shape is limited to being depicted as cylindrical, and the distribution of particles is shown as a simple cubic lattice. However, the highest density package a simple cubic lattice can achieve is 52 vol.%, which is insufficient for obtaining viable calculations since actual particles will congregate at more than this density level in a composite.

To address the deficits of a two-dimensional model of a composite material, advanced computer calculations have facilitated the development of a more useful 3D model. In order to ensure that the structure can be repeated, a crystal system has been applied to describe a magnetic composite. There are three common cubic bravais lattices: simple cubic lattice (s.c.), body-centered cubic lattice (bcc) and face-centered cubic lattice (fcc). The structures of the three lattices are showed below in Fig. 9.

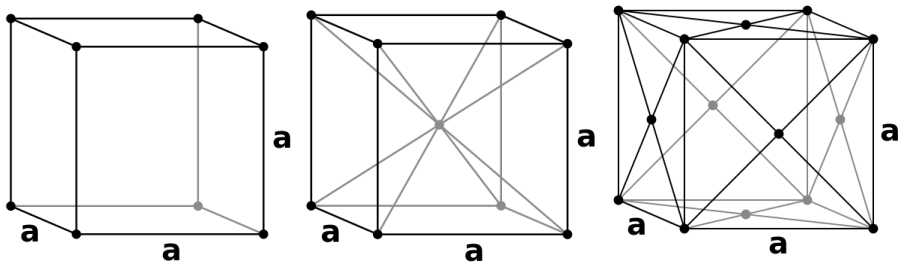

(a) (b) (c)

Fig. 9. Structures of the three most common cubic bravais lattices (a) simple cubic lattice (s.c.), (b) body-centered cubic lattice (bcc), and (c) face-centered cubic lattice (fcc) [34].

The maximum volume percentage of particles in a given lattice will occur when the particles are in contact with each other. Suppose the shape of particles in a magnetic powder is supposed to be spherical. The maximum volume percentages of each of the three kinds of lattice are shown in the

TABLE 1.

TABLE 1. Volume percentage of particle in the lattice in the simple cubic lattice (s.c.), body-centered cubic lattice (bcc), and face-centered cubic lattice (fcc).

	s.c.	bcc	fcc
Volume of the lattice	$8r^3$	$\frac{64\sqrt{3}}{9}r^3$	$16\sqrt{2}r^3$
Number of particles in one lattice	1	2	4
Volume percentage of particle in the lattice	$\frac{\pi}{6}$ (52%)	$\frac{3}{8\sqrt{3}}\pi$ (68%)	$\frac{1}{3\sqrt{2}}\pi$ (74%)

For the magnetic material we fabricated, the volume faction was always between 45 vol.% and 55 vol.%. However, the simple cubic lattice cannot attain this volume percentage level, and this level is insufficient for the face-centered cubic lattice. In contrast, based on the work of Hashemifard [35], who successfully utilized the body-centered cubic lattice crystal structure as a model of permeability for a mixed matrix membrane (MMM), we also decided to employ the bcc lattice as the base unit cell. It must be noted, however, that utilizing the bcc lattice with particles of the same diameter results in the loss of accurate information about particle size distribution; moreover, there are many tiny particles in the structure that are not included in the average size counting. Additionally, the particle-to-particle distance is too large in the model when the volume percentage is 50% in bcc, which is 0.56r (r is the average radius of the magnetic particle). Although such a large gap may be observed in the resulting micrograph, it is unlikely to impact the properties of a composite material.

Thus, we incorporated smaller particles in our new FEA model. Based on the fact that a composite is a homogenous material, the smaller-sized particles should uniformly distribute

within the unit cell—meaning that they would disperse somewhat regularly between each of two larger particles. Recall that tiny magnetic particles are too small to count in an experimental micrograph in comparison to regular particles. Indeed, the diameter of tiny particles can essentially be undetectable. Therefore, by obtaining an average between the size of regular particles and the size of tiny particles, the size of small particles can safely be determined as half of diameter of the regular particle.

Moreover, this FEA model was used to calculate electromagnetic properties only—meaning that the air bubbles and the polymer material are essentially indistinguishable in terms of their individual property impacts. For instance, the relative permeability of both are one, implying that neither contributes to core loss density. In other words, the air bubbles are ignored in this model. The 3D structure of a unit cell of a magnetic composite material is shown in Fig. 10, where blue particles are magnetic particles and white spaces represent the polymeric material.

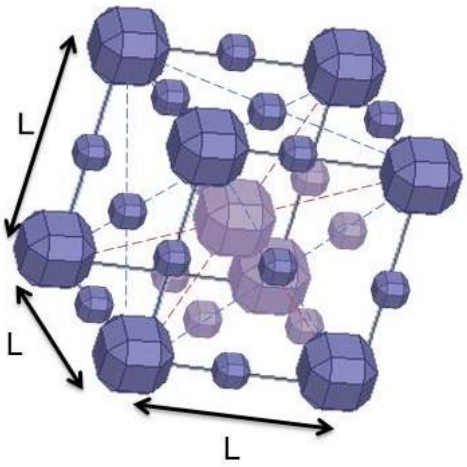

Fig. 10. An example of a model of a polymer matrix-metal composite.

In summary, this chapter introduces a new FEA model to describe the relationship between the constituent components of a magnetic composite and magnetic calculation. The model presented herein includes two materials: magnetic powder particles and a polymer binder. In one model, there are two large particles and six small particles. As described in the aforementioned equations, there are two important factors that impact the permeability of the composite: shape factor (A_w), volume factor (a). With respect to the former, its impact is highly dependent on the shape of the materials. In terms of the influence of volume, it is controlled by the particle-to-particle gaps (g). Assuming that all the particles are spherical in shape, and the smaller ones have a diameter of "*D*", therefore, the radii of the large particles are "*D*", while the volume factor is:

$$a = \frac{4\pi D^3}{L^3} \tag{9}$$

where *L* is the length of the unit cell, which can be determined by equation (10)

$$L = 3D + 2g \tag{10}$$

Additionally, the weight percentages can also be derived by determining the density of magnetic materials and polymers.

In addition to the incorporation of magnetic particles, flakes can also be introduced into the experimental composite as well as into the model structure. The flake dimensions for the model assay were determined by experimental results. In order to simplify the model structure and reduce calculation memory, the thickness and length of flakes must be identified. The width, however, is dependent upon the volume fraction of flakes in the composite. The distribution of powder particles follows a "body-centered cubic" structure. Since flake length is always larger

than the side length of a unit cell, multiple unit cells are applied in the polymer matrix-magnetic-particle-flake composite. A model example is shown in Fig. 25 (Chapter 4).

Chapter 3. Simulating properties of BCB matrix-permalloy composites from FE simulation

This chapter details the development of a model of a particular polymer matrix-metal composite. Specifically, the polymer in the model is Benzocyclobutene (BCB) and the magnetic metal is a permalloy powder. Chapter 3 begins with an overview of magnetic materials and the rationale for choosing permalloy. A unit cell of the composite is described and the properties of the model are explained. Additionally, in order to determine the accuracy of the model, an experimental approach was designed for measuring the properties of the composite. As detailed herein, our experimental results were analogous to those obtained via simulation. Finally, this chapter closes with a discussion of the modulation of the weight percent of magnetic powder on the properties of the resulting composite.

3.1 Introduction of permalloy

When applied to the field of power electronics, magnetic materials can be classified as either hard or soft. Soft magnetic materials can be easily magnetized and demagnetized at relatively low magnetic field value, since these compounds typically feature relatively low coercive force H_c. In terms of industrial applications, soft magnetic materials are widely utilized in resonance inductors, high frequency transformers, and so on [36].

Soft magnetic materials are classified into four categories: ferrites, iron alloys, amorphous alloys, and nanocrystalline materials [37]. Of particular interest to this investigation are the iron alloys

features higher saturation flux densities and Curie temperatures in comparison to the ferrite varieties. Iron alloys can be divided into silicon steel and iron-nickel (FeNi) alloys. The former, which was introduced earlier into inductors and transformers, has a high saturation flux density but is brittle. FeNi alloys display the highest initial relative permeability values, which can reach up to 100,000 (μ_i), as well as high saturation flux density, which can reach 1.6T. The most important FeNi alloys for industrial purposes are permalloy (20% iron and 80% nickel), 78Ni-Fe alloy (22% iron and 78% nickel), Orthonol (50% iron and 50% nickel), and supermalloy (an improved permalloy composed of 75% nickel, 20% iron, and 5% molybdenum). A summary of the magnetic properties of iron alloys is provided in TABLE 2.

TABLE 2. Magnetic properties of iron alloys material [38].

Materials	Composition	Initial permeability μ_i	Flux density B_{max} Tesla	Curie temperature ℃	dc, Coercive force, H_c Oersteds
Silicon steel	3% Si 97% Fe	1,500	1.5-1.8	750	0.4-0.6
Orthonol	50% Ni 50% Fe	2,000	1.42-1.58	500	0.1-0.2
Permalloy	79% Ni 17% Fe 4% Mo	12,000-100,000	0.66-0.82	460	0.02-0.04
Supermalloy	78% Ni 17% Fe 5% Mo	10,000-50,000	0.65-0.82	460	0.003-0.008

3.2 Modeling of BCB matrix-permalloy composites

To reiterate, permalloy (Ni-Fe-Mo) features high relative permeability and low coercive force. The former is important for composite fabrication, while low coercive force is link to reduced hysteresis loss and increased sensitivity to a magnetization field. Given these property parameters, a mixture of a polymer and permalloy powder can help increase saturation flux density and electrical conductivity. Specifically, high saturation flux density broadens the application of the magnetic material to higher current and increasing electrical conductivity significantly decreases eddy current loss at high frequencies. The following section will discuss the specific properties of permalloy, the model structure of the polymer matrix-permalloy composite, and the computational set-up we utilized to evaluate the properties of the composite.

3.2.1 Physical properties of permalloy powder

For this investigation, the permalloy 80 from ESPI METALS was used to conduct our simulation; this permalloy powder was also utilized in actual experimental conditions. In order to design the structure of our model structure, the size of the permalloy powder was required.

To simplify the model structure of the powder, the sphere is assumed to be the shape of each particle. The morphology of the powder in the polymer matrix-metal composite is shown in Fig. 11, where the size of each particle is illustrated in the micrograph; this figure represents a cross-section of a BCB matrix-permalloy composite obtained via SEM. Since the diameters of the particles are random variables with an unknown distribution, it is suitable for normal fit. The normal fit of the diameter distribution of permalloy particles is illustrated in Fig. 12.

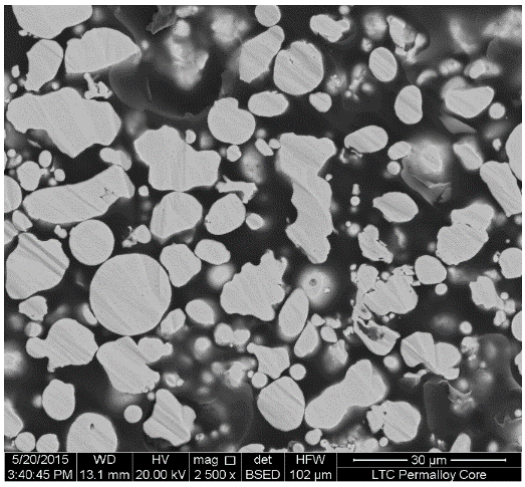

Fig. 11. Micrograph of a cross section of BCB matrix-permalloy composite.

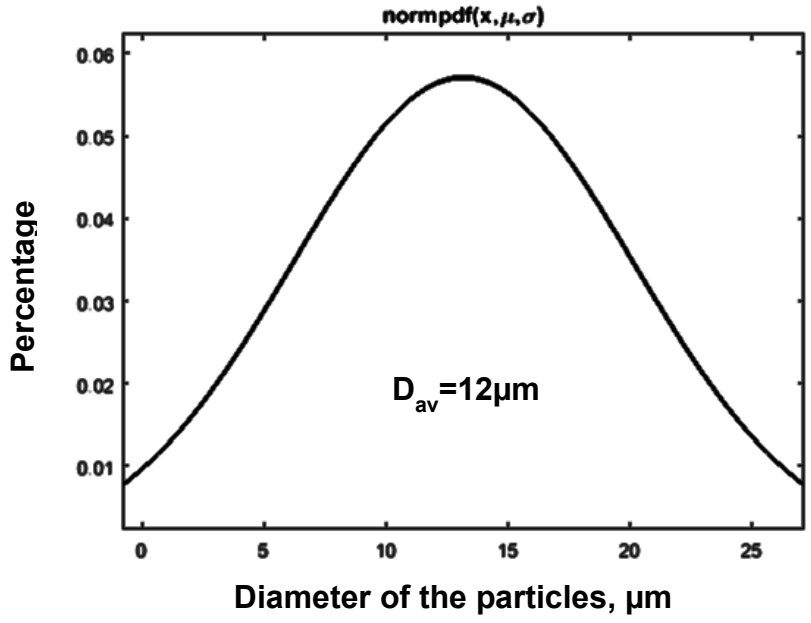

Fig. 12. Norm fit of diameters (D) of permalloy particles.

Based on the normal fit results shown in Fig. 12, it is clear that the average diameter is around 12 micrometers. Thus, the particle structure model should resemble a ball whose diameter is equal

to 12 micrometers. However, we encountered a problem that must be noted: curved surfaces that are densely meshed will require a significant amount of computer memory and could thus impede the resulting calculations. Moreover, 3D simulations always require much more memory than 2D simulations. Consider also that this model is somewhat complicated - meaning that when sphere particles are used, the required computer calculation ability is higher thereby increasing the risk of stalling due to memory shortfalls. However, the alternative of using the cube to describe the particles will not be amenable to analyses of the flux in the composite model which is possible when incorporating spheres in the model.

As a viable alternative, a polyhedron was utilized to describe the particle shown in Fig. 13. In terms of software modifications, we were able to create it by shaving the corners and edges of a cube, wherein each side is the same as the diameter of the spheres. The cut represents a quarter of the length of each side. As mentioned before, the shape of the particle will influence the properties of the composites. Based on equations (3) and (4), since the length in parallel and across of flux is the same in the new structure, the A_w of the new particle shape is the same as the sphere. Therefore, selecting the new shape instead of the sphere is likely to exert little impact on the accuracy of resulting data.

By replacing the magnetic particles described in Chapter II with permalloy particles, the structure of polymer matrix-permalloy composites could be determined.

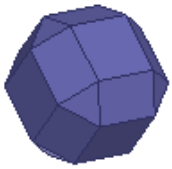

Fig. 13. The shape of permalloy powder.

ANSYS Maxwell, which is electromagnetic field simulation software, was utilized conduct the simulation experiment described herein. First, in order to calculate the flux distribution, the magnetization ability in response to the magnetic field is required. In other words, the magnetic properties of a given magnetic material are required in modeling studies. For the polymer, a benzocyclobutene (BCB) insulating layer is applied whose relative permeability is 1; as such, the polymer does not experience any core loss effect since its resistivity is infinity and has no magnetization effect. The density of BCB is 1 g/cm^3.

The ESPI Metals company lists some of the magnetic properties (TABLE 3) and the physical properties (TABLE 4), shown below.

TABLE 3. The magnetic properties of permalloy 80 from ESPI Metals [39].

Maximum permeability μ_i	Permeability (B=100) μ_i	Coercive force A/m	Saturation flux density Tesla	Residual induction Tesla	Resistivity $\Omega - cm$
300,000	75,000	1.2	0.75	0.37	10-100

TABLE 4. The physical properties of permalloy 80 from ESPI Metals [39].

Density ρ g/cm^3	Electrical resistivity $\Omega - cm$	Thermal conductivity Cal/cm^3/sec/℃	Specific heat Cal/g/℃	Thermal expansion in/in/℃
8.74	58	0.047	0.12	12×10^{-6}

The company, Magnetics, tested the core loss density of permalloy flakes at different thicknesses. Fig. 14 illustrates the core loss density of permalloy flakes versus flux density at ¼ mile. There are two significant losses in the permalloy that should be considered. The first is the hysteresis loss which should be slightly lower with powder in comparison to flakes, since the powder shape has lower coercivity [40]. The other significant loss pertains to changes in the eddy current in the eddy current. Ideally, eddy current loss should be two dimensional circles, but because the thickness of flakes is the same as the diameter of the particles, the maximum diameter of eddy current is the same between both sphere particles and flakes. While there is no significant difference, the use of Steinmetz equation [41] from permalloy versus flake shaped can estimate the loss of permalloy in the sphere shaped particles.

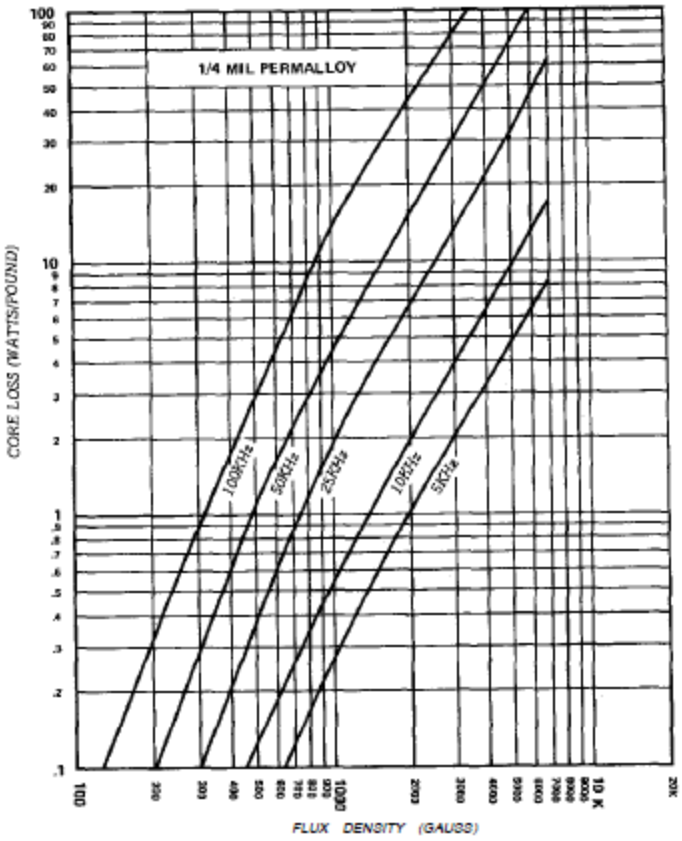

Fig. 14. Core loss density of permalloy powder of permalloy 80 from Magnetics [42].

3.2.2 Structure of the model of BCB matrix-permalloy composites

Recall that the structure of our body-centered cubic model is described in Chapter II. In As noted earlier, there are two dimensions that need to be specified in the creation of such a model. One is the size of the particles (discussed in Section 3.2.1), and the other is the side length of the body-centered cube. The side length of the cube includes one diameter of a large particle, one diameter of a small particle, and two particle-to-particle gaps, which is determined by the weight percent

of each component in the composite. For this investigation, the weight percent of permalloy in the composite was 90% and the two particle-to-particle gaps were $0.1\mu m$ each.

3.2.3 Excitation of the model in simulation

The purpose of a simulation is to determine the properties of the magnetic material – i.e., how the magnetic materials respond to a magnetization field, which can be applied in two ways: (1) adding a direct current to the model, and (2) adding a magnetic field (H field) to the model.

Adding a direct current to the model represents a traditional methodology of calculation the properties of inductor components. In order to use this approach, one must model the number of turns of windings, which do not, however, impact the properties of the magnetic material. Instead, by adding a current to each turn of windings and setting them in series, the magnetic field (H field) will be generated. This method, then, calculates the magnetic properties from inductor properties: The inductance of the inductor derives the permeability of the magnetic material (Eq. (11)). Additionally, the core loss of the inductor is equivalent to the loss of the magnetic material.

$$L = \frac{\mu N^2 A}{l} \tag{11}$$

In Eq. (11), L is the inductance of the inductor, $\mu = \mu_0 \mu_r$ is the permeability of the magnetic material, μ_0 is the permeability constant which equal $4\pi \times 10^{-7}$, μ_r is the relative permeability, N is number of turns, A is cross section area of the core, and l is the main length of flux length in the core.

Although this method works well for bulk materials with high permeability, there is a problem when assessing composite material. Specifically, the ANSYS Maxwell calculates software the inductance level from the energy storage which can be represented as:

$$W_m = \frac{1}{2} L i^2 \tag{12}$$

where W_m is the stored energy in the whole calculation region; L is the inductance; and i is the current in the winding [43]. Given the fact that the relative permeability of the polymer in the composite material is the same as in the air (namely, 1), there is a significant level of energy stored in the air (out of the core). In other words, the inductor material will add a lot of ambient air, which causes the calculated permeability to be lower than actual permeability.

The second approach for exciting a model in simulation is to add a magnetic field (H field) to it. In this method, one piece of magnetic material is directly added to a magnetic field. The ANSYS Maxwell software can then determine the average value and the direction of the magnetic field.

In this excitation, permeability can be calculated using the definition shown in Eq. (13), while the core loss density value represents the loss of the whole calculation region.

$$\mu = \frac{\bar{B}}{\bar{H}} \tag{13}$$

In Eq. (13), $\bar{B}$ is the average flux density and $\bar{H}$ is the average magnetic field.

This second approach is much easier to analyze and calculations from the definition are significantly more accurate.

As a result, the second excitation method is preferred for this investigation. This excitation is set by boundary condition. Next section will talk about boundary condition.

3.2.4 Boundary condition of the model in simulation

In order to implement the second excitation method, the boundary condition, which exists on the surface of the calculation region, represents an important parameter to consider.

First, the boundaries cannot overlap with the surface of the model. When the boundary is established, the boundary fields must be the same as the boundary conditions. If the boundaries overlap with the surface of the model, the field on the surface will be impacted by the boundary condition.

Secondly, the boundary conditions on the side surfaces of the calculation region should be straight from bottom to top, which is parallel to the surface. Additionally, the average value set on the four faces must be the same. The magnetic field strength will change according to the calculated core loss density at different peak-to-peak flux densities (B_{ac}). In a BCB matrix-permalloy composite unit cell, when the added H field is 15 A/m sinusoidal waveform, the average Bac is 10 mT.

Finally, the boundary conditions on the top and bottom surfaces of the calculation region should be perpendicular to the surface. The directions should be kept the same: from bottom to top. And the average value is the same as the second step. It should also be noted that the permeability of the region between the boundary and the model should be zero to help the flux concentrate in the model.

3.2.5 Mesh assignment to the model

Utilizing finite element analysis (FEA), the size of mesh directly decides both accuracy and speed. When a mesh is too coarse, the calculation may end up as “not convergent,” even after ten

iterations. When the a mesh is too fine, the calculation is likely to require a great deal of computer memory—with the risk of running short of memory before the calculation has been completed. The choice of mesh size usually depends on direct experience. To optimize speed and accuracy, engineers usually set the mesh to be relatively coarse at the surface and finer at the corners. In a BCB matrix-permalloy composite, the length of the mesh is 0.005 mm in the unit cell, while the size of the surrounding mesh is determined automatically due to the fact that the structure in one unit is much more complicated than its surroundings.

3.3 Computation results and discussion

This section reports our computational results, and then compares them with analogous experimental measurements obtained in our lab—with a particular focus on two essential magnetic properties addressed in this thesis: permeability and core loss density.

3.3.1 Experimental measurement of the properties of magnetic material

To test the magnetic material properties of our simulation composite, an actual composite material, BCB matrix-90wt.% (56vol.%) permalloy composite, was fabricated in our lab. As shown in Fig. 15 and Fig. 16, we utilized a Keysight (Agilent) 4294A (Fig. 15) impedance analyzer with a Keysight 16454A fixture (Fig. 16). The core has to be toroid shaped to be inserted into the fixture, and the fixture featured a one-turn winding. After calibrating the equipment and the fixture, the complex permeability equation was drawn on the screen, as follows:

$$\mu = \mu' - j\mu" \tag{14}$$

where μ' is the real part of permeability and $\mu"$ is imaginary part of permeability. The real part of permeability is aforementioned relative permeability, while $\mu"$ represents the loss of the magnetic material.

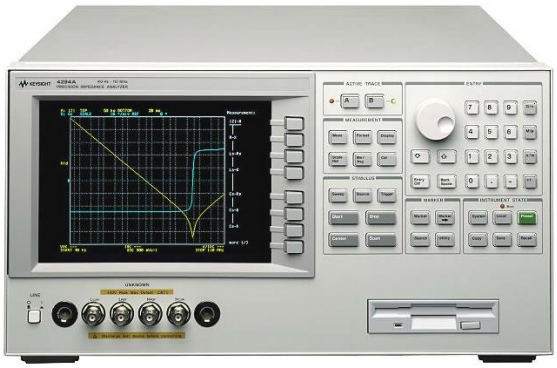

Fig. 15. Impedance analyzer to test the relative permeability of the core [44].

Fig. 16. Keysight 16454A fixture to test the complex permeability of the core [45].

The loss calculated from simulation is the core loss density, rather than the imaginary portion of permeability. Therefore, an assessment of core loss density is required. The setup we utilized

followed a previously established method reported by Mingkai Mu [46]. The topology of the core loss density measurement is designed in Fig. 17. A toroid core was fabricated using the test magnetic composite material, and then later wound using Litz wires as a transformer. The cap C_r was a resonant capacitor to cancel the imaginary portion of complex impedance of the transformer. As a result, the voltage (v_3) across the transformer and the resonant capacitor (Cr) was found to be in phase with the current, which affords excitation to the transformer. In the circuit, the current flows from the voltage source to the primary side of the transformer and resonant capacitor, and the voltages are tested from the secondary side of the transformer to remove the test effect on the power stage as shown in Fig. 17.

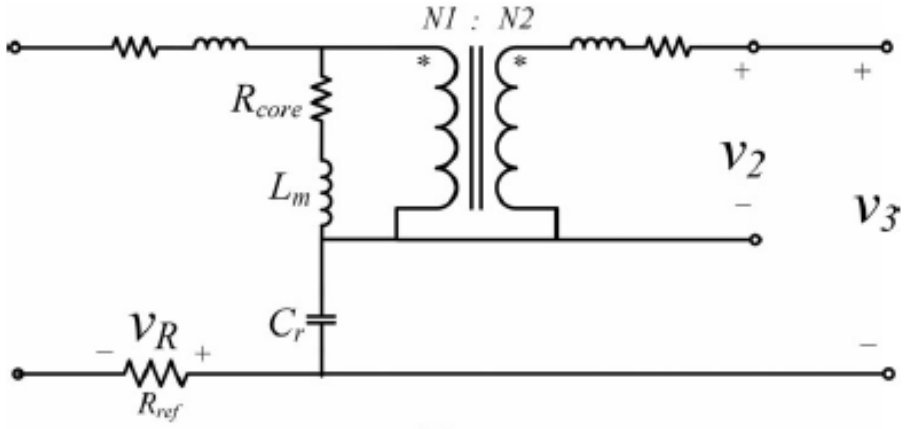

Fig. 17. Equivalent circuit to test the core loss density of the core at different magnetic field ($N_1 = N_2$) [46].

Fig. 18 shows an example of the tested waveform from the setup. The current through the resonant bench is represented by the voltage across the sense resistor (R_{ref}). The voltage across the resonant bench (v_3) and the voltage across the sense resistor (v_r) are 180° in phase.

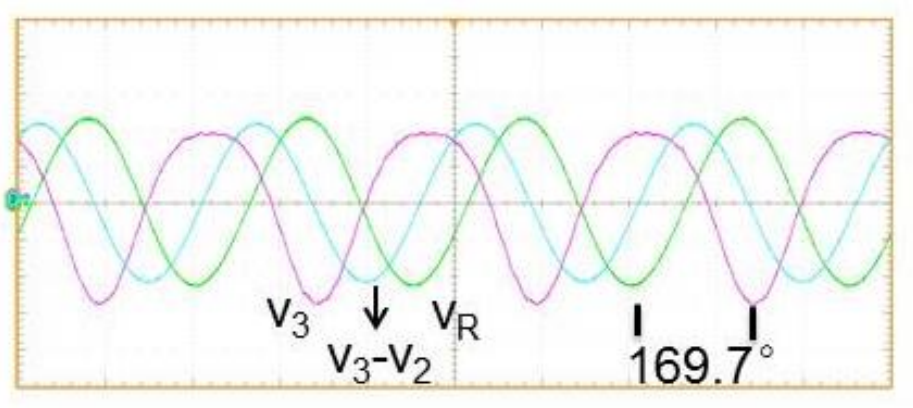

Fig. 18. Waveform from the core loss density measurement setup [46].

From Steinmetz equation[41], the core loss density can be expressed by

$$P_v = C_m f^a B_{ac}^{\beta} \tag{15}$$

where P_v is core loss density of magnetic material; C_m, α, and β is a constant; f is frequency; and B_{ac} is half of the peak to peak flux density. It is clear that flux density is a factor in the resulting core loss density level.

The core loss density can be calculated by the equation below.

$$P_v = \frac{1}{TR_{ref}} \int_0^T v_3 v_r \, dt \tag{16}$$

where T is the time of one cycle.

Flux density can be calculated by

$$B_{ac} = \frac{1}{N_2 A_e} \int_0^T v_2 \, dt \tag{17}$$

where N_2 is the number of turns in the secondary side; A_e is the cross area of the toroid core; and v_2 is the voltage across the transformer.

In summary, the core loss density of the composite material can be tested by the setup in a toroid shape.

3.3.2 Comparison of permeability between simulation and experiment

This section will discuss the permeability calculated by our FEA model utilizing the ANSYS Maxwell software, in comparison to results obtained by the impedance analyzer.

In our simulation assay, the weight or volume percent of permalloy powder in the composite was easy to change by adjusting the particle-to-particle distance. The volume percent of permalloy powder and relative permeability of the core is depicted in Fig. 19.

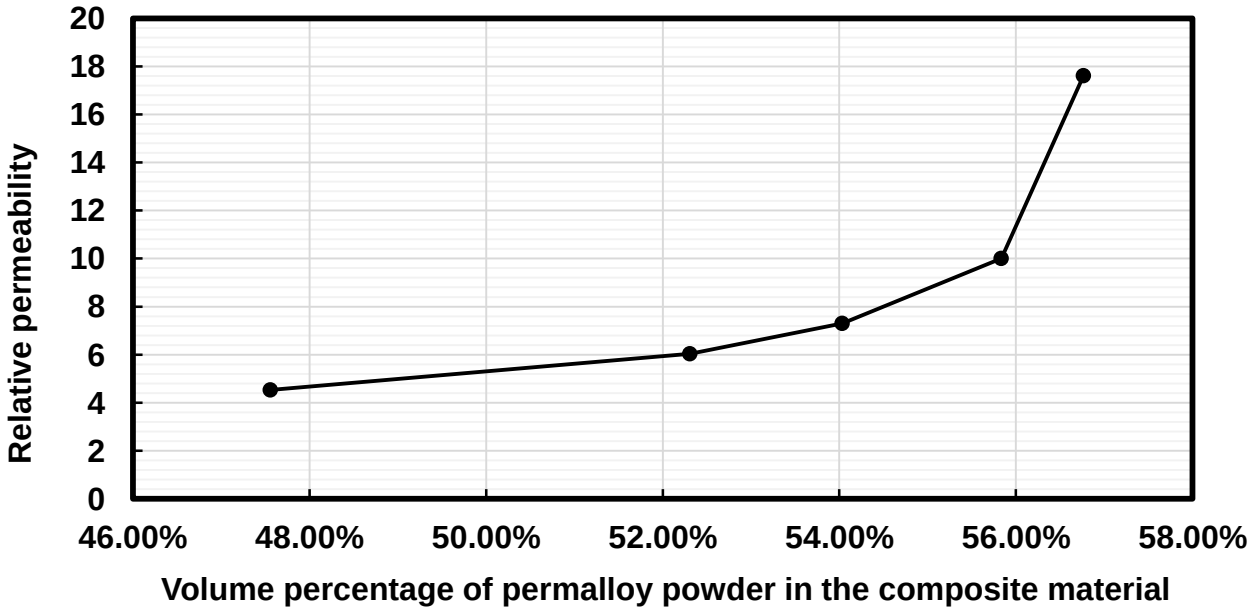

Fig. 19. Volume percentage of permalloy powder effects on the relative permeability of the core.

From Fig. 19, it is clear that the relative permeability will increase when the volume percent of permalloy powder increases, as well as the slope of permeability. This relationship stems from the fact that reluctance is low in the permalloy particles, but high in the BCB. Furthermore, a higher volume percentage means smaller gaps between the permalloy particles, which decreases the reluctance of the whole model and increases the permeability. Also, increasing the percentage at a higher volume percent means a reduction in the volume of BCB at a relatively lower level, which reduces the gaps between particles at a relatively smaller value. Thus, at high volume percentage of permalloy particles, the permeability will increase much quicker than at a low volume percentage.

Based on simulation results, it appears that relative permeability can escalate up to 75,000 (the relative permeability of bulk permalloy). In reality, however, this level is not possible. The 57 vol.% permalloy is the highest volume percent the experiment can achieve; beyond that point, the material will easily crack when cured.

As for our experimental results, recall that we synthesized the BCB matrix-90wt.% (56vol.%) permalloy composite material and measured it via an impedance analyzer. Our measurements confirmed that there was little vibration at low frequency and the relative permeability value prior to reaching the resonant frequency was 10. Thus, the relative permeability of BCB matrix-90wt.% (56vol.%) permalloy in simulation was 10, which agrees with our experimental findings.

3.3.3 Comparison of core loss density between simulation and experiment

This section summarizes our comparison study of core loss density calculated by the FEA model using the ANSYS Maxwell software, and the analogous findings obtained via the

aforementioned experimental setup. Also reported in this section are the weight percentage findings based on the permalloy powder effect. In Utilizing Maxwell, the eddy current mode can simulate core loss density at different peak-to-peak flux densities (B_{ac}). For instance, sweeping the magnetic field from 15 A/m to 37.5 A/m, the B_{ac} will change from 4 mT to 10 mT. By measuring the core loss density of BCB matrix-56 vol.% permalloy utilizing a previously reported method [46], we were able to produce the plot shown in Fig. 20. The red line measures actual experimental core loss density values, while the black line provides analogous values for our simulation study. As shown, the experimental core loss density values were larger than the simulated values. There are two possible reasons for this discrepancy:

1. The material properties are not accurate. Because the data obtained from Magnetics was published in 2000 (see Fig. 14), those measurements may not be sufficiently precise.
2. The magnetic field is not uniform in the toroid core, which we then incorporated in our experimental study. In the simulation, only one unit cell was simulated. In other words, this approach assumes that the magnetic field was uniform in the material. However, it is well known that the toroid core features a higher magnetic field in the interior compare to the exterior.

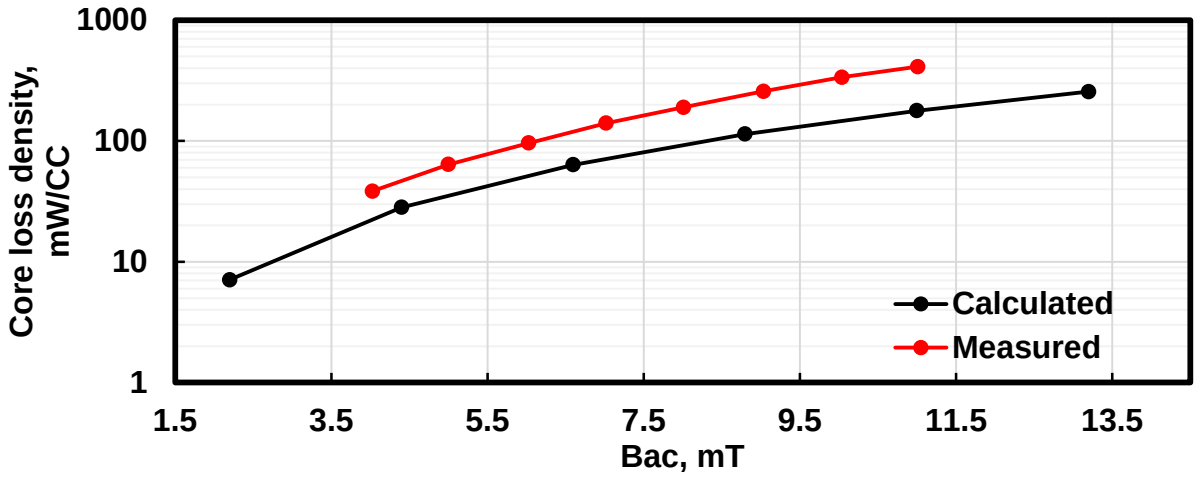

Fig. 20. The comparison between the measured and the calculated core loss density of BCB matrix-permalloy core at 1 MHz.

Although we noted some differences between the results we obtained for the simulation and experimental studies, the tendency of the core loss density values changing with weight (volume) percentage remained consistent. Fig. 21 illustrates how the volume percentage of permalloy powder affects the core loss density of the composite. As shown on the graph, increasing the volume percentage of permalloy powder increases not only the permeability, but also the core loss density. This correlation is due to the fact that when the volume percentage increases, the particle-to-particle distance decreases, which will introduce an inhomogeneous factor. Consider the example of two composites—one is 55.8 vol.% (91.7 wt.%), and the other is 47.6 vol.% (88.8 wt.%). The particle-to-particle gap is 0.1μm in the 55.8 vol.% composite, but is 0.6μm in the 47.6 vol.% composite. An examination of a cross-section of the unit cell reveals that there are five paths along which the flux can travel (as shown in Fig. 22). The length of the polymer in each path is listed in TABLE 5. The reluctance of each path is represented as:

$$R = \frac{l}{\mu A} \tag{18}$$

where R is reluctance; μ is the permeability of the path; l is length of the path; and A is a cross-section of the path. Because the permeability of permalloy ($\mu_r = 75000$) is much larger than the polymer ($\mu_r = 1$), the polymer is dominant in reluctance. We calculated the reluctance for each path with the same cross-section area, assuming that the reluctance of the path 1 was R. Comparison data is provided in TABLE 5. As shown in this table, compared to the 47.6 vol.% composite, there was greater difference reluctance in the 55.8 vol.% composite. As a result, the flux is more inhomogeneous in the 55.8 vol.% composite which can also be seen in Fig. 23. The inhomogeneous distribution of flux density means that the particles along the path of shortest distance represent the primary source for loss dissipation in the model.

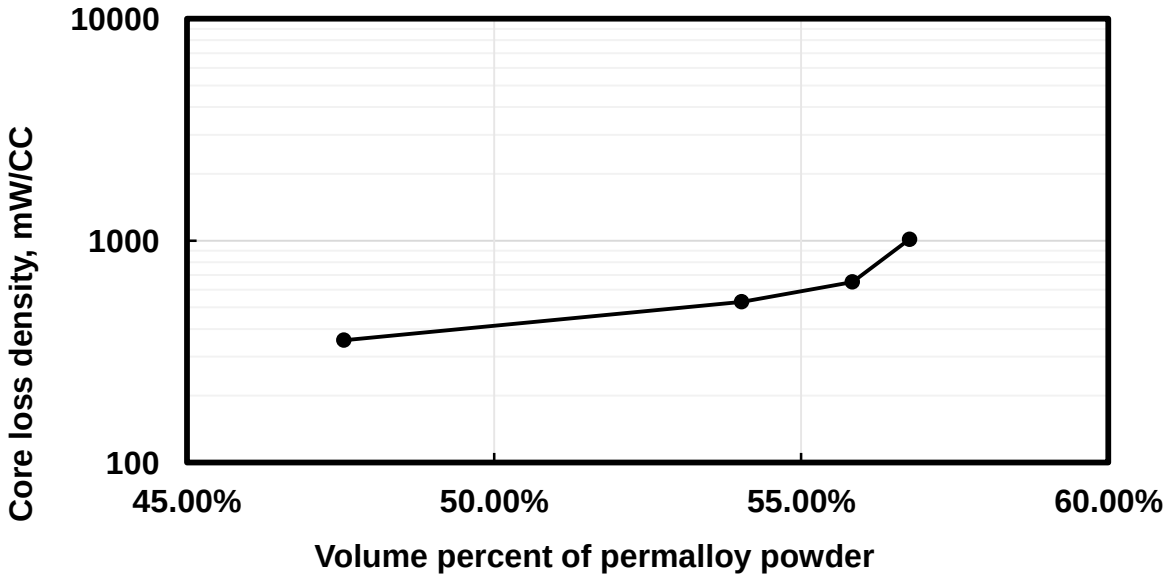

Fig. 21. Volume percentage of permalloy powder effects on the core loss density of the core at Bac=4 mT, 1 MHz.

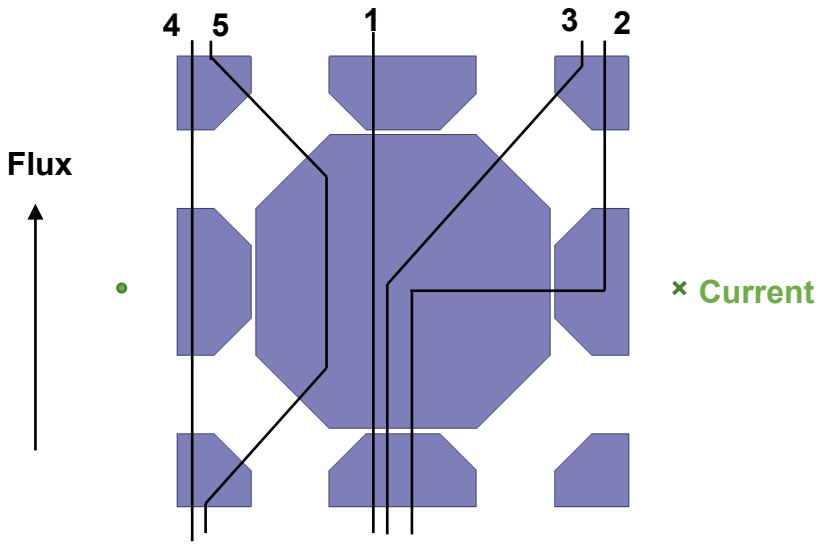

Fig. 22. One cross section of the unit cell.

TABLE 5. Comparison between the reluctance at different volume percentages.

	Volume percentage of composite	Flux paths in each composite				
		1	2	3	4	5
Length of polymer in the path	55.8 vol.%	0.2μm	3.3μm	3.4μm	6.2μm	6.6μm
	47.6 vol.%	1.2μm	4.8μm	4.6μm	7.2μm	8.1μm
Reluctance	55.8 vol.%	$R_{56\%}$	$16.5R_{56\%}$	$17R_{56\%}$	$31R_{56\%}$	$33R_{56\%}$
	47.6 vol.%	$R_{48\%}$	$4R_{48\%}$	$3.8R_{48\%}$	$6R_{48\%}$	$6.8R_{48\%}$

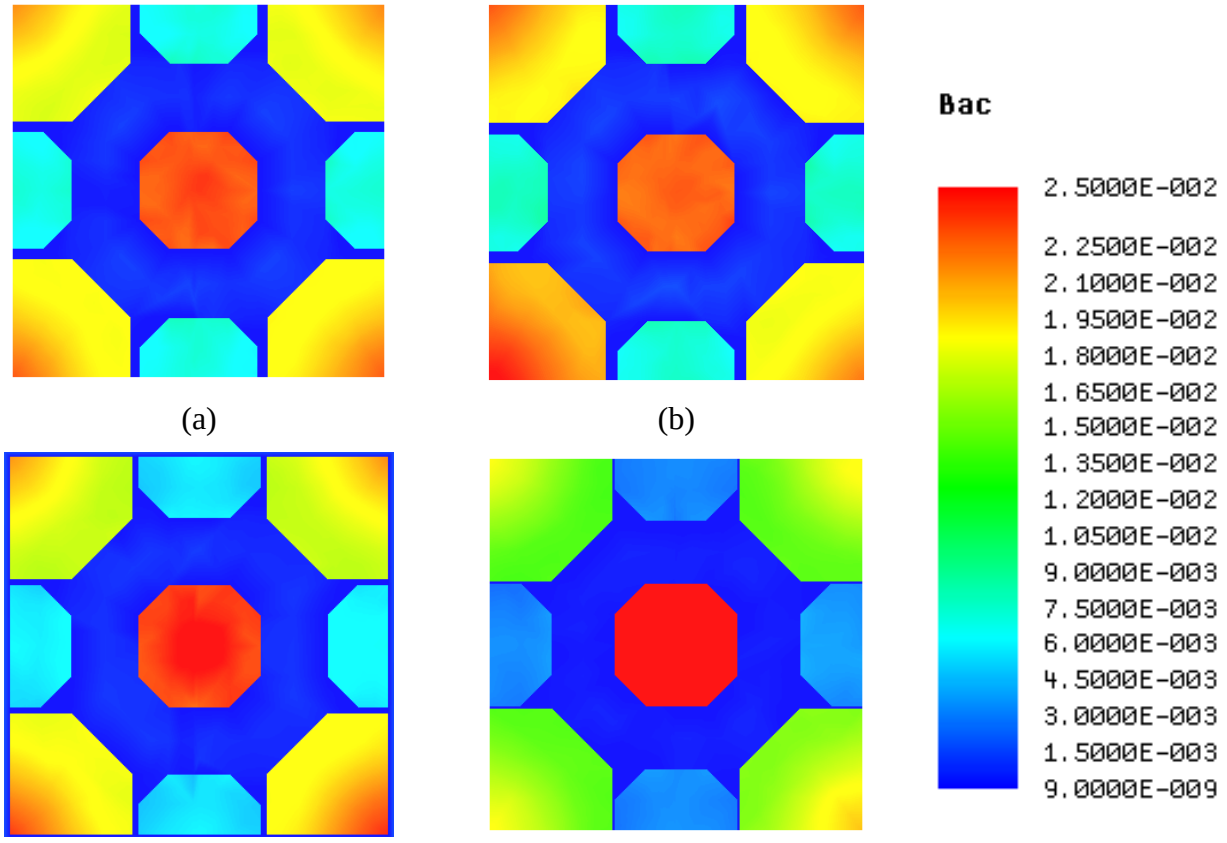

Fig. 23 Flux density distribution at different volume fraction of magnetic particles (a) 47.6 vol.%, (b) 49.1 vol.%, (c) 52.3 vol.%, and (d) 55.8 vol.%.

As described in this chapter, BCB matrix-permalloy composites were simulated and measured. In this model, the relative permeability agreed with analogous experiment data. It must be noted, however, that some discrepancy in core loss density values was noted between the simulation and experimental models.

Chapter 4. The effects of Metglas flakes in magnetic composites

As discussed in Chapter 3, a BCB matrix-permalloy composite was both simulated and measured experimentally. To optimize the properties of a given magnetic composite material, we designed this investigation to compare the relative merits of incorporating two different kinds of magnetic components in our BCB-based composites: permalloy powder and Metglas flakes. While the effects of incorporating a permalloy powder are detailed in Chapter 3, this chapter discusses the incorporation of Metglas flakes, with a particular emphasis on the impact of flake thickness on magnetic properties.

4.1 Introduction of Metglas

As mentioned in Chapter 3, soft magnetic materials are typically classified into four categories: ferrites, iron alloys, amorphous alloys, and nanocrystalline materials [37]. Metglas belongs in the category of an amorphous alloy, which is a non-crystalline metal alloys. An amorphous alloy is characterized by high saturation flux density (above 1.6T) and high relative permeability (up to 80,000). In general, the electrical resistivity and Curie temperature of an amorphous alloy can reach 16μΩm and 460°C, respectively. Since amorphous alloys feature low coercive force, they are sensitive to small-applied magnetization fields.

4.2 Modeling of BCB matrix-permalloy-Metglas composites

To reiterate, Metglas is characterized by high permeability, which is enhanced by its flake-shaped configuration. The Metglas used in this investigation was Metglas 2705M. TABLE 6 lists

the physical properties of the Metglas 2705M flakes as provided by the company. It must be noted, however, that the thickness of flakes in the model is thinner than shown in their datasheet. This discrepancy is due to the fact that the flakes in our composite material were inserted after ball mill grinding.

TABLE 6. The physical properties of Metglas 2705M from Metglas [47].

Density ρ g/cm^3	Electrical resistivity $\mu\Omega - cm$	Thickness μm	Thermal expansion ppm/℃
7.8	136	22	12

This section will focus on simulation structure results. In terms of the modeling setup for this phase of the investigation, it is analogous to the setup for BCB matrix-permalloy composites described in Chapter 3.

4.2.1 Description of model structure of flakes in the composite

With respect to important characteristics involved in modeling BCB matrix-permalloy-Metglas composites, it must be noted that the structure of permalloy maintains the body-centered cubic model, into which the flakes are inserted. Since the flakes are much larger than permalloy powders, multiple powder unit cells are used for one unit cell of a BCB matrix-permalloy-Metglas composite. Moreover, the incorporation of flakes will inevitably cut the powder particles in the model, so there will be some small particles, which is confirmed by micrograph results.

To measure the properties of the BCB matrix-permalloy-Metglas composite, a toroid core was obtained, which was then cut and cross-section SEM results were obtained. The micrograph is shown in Fig. 24 (a). The distribution of length and thickness of flakes are shown in Fig. 24 (b)

and Fig. 24 (c), respectively. The average length of the flakes was 192 μm and the average thickness of flakes was 21.3 μm. The width of the flakes was determined by calculating the weight percent of Metglas flakes in the composite material.

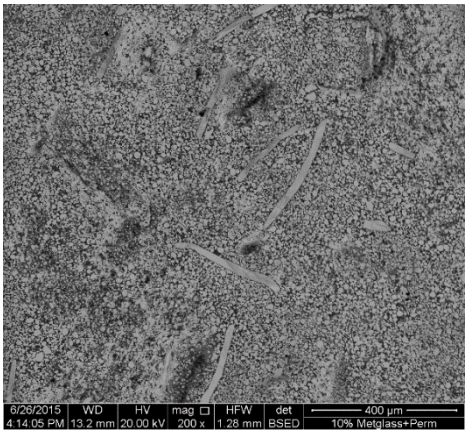

(a)

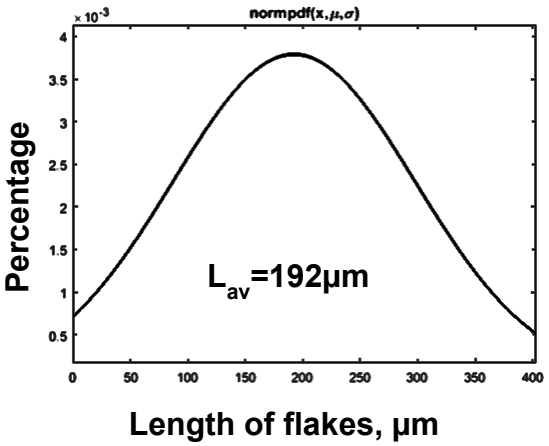

(b)

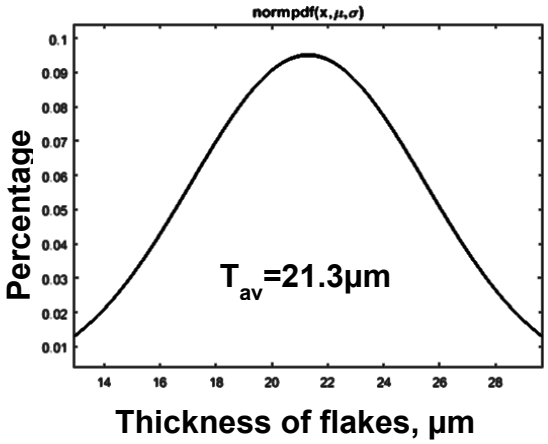

(c)

Fig. 24. Dimensions of Metglas flakes in the composite. (a) is the SEM micrographs of BCB matrix-permalloy-Metglas composite. (b) and (c) are the dimensional results of the flakes.

As for the particle-to-particle distance from the micrograph—it is the same in both modeled BCB matrix-magnetic composite.

It must be noted that the amount of Metglas flakes in the composite material can be up to 12.5 wt.%. So, using the example of a model structure of a 12.5 wt.% BCB matrix-permalloy-Metglas, the magnetic material is 90 wt.% percent in the composite, and the Metglas is 12.5 wt.% of the magnetic material. Based on weight percentages and densities, the structure of the composite is shown in Fig. 25. The part shaded in green represents a piece of Metgals flake; the blue particles depict the permalloy powder; the yellow winding is copper wire; and the blank space is the polymeric material.

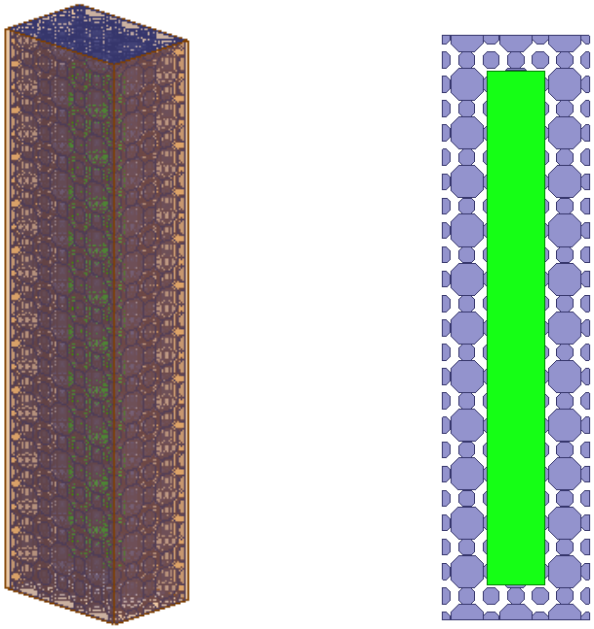

(a) (b)

Fig. 25. Model of BCB matrix-permalloy-Metglas composites. (a) 3D structure of the model (b) cross-section of the model.

4.2.2 Magnetic properties of magnetic flakes in the composite

In order to simulate the material utilizing the ANSYS Maxwell software, two pieces of information are essentical: the geometry of the material and its magnetic properties. The data of magnetic properties were obtained from the Metglas website and are shown TABLE 7 and Fig. 26.

TABLE 7. The magnetic properties of Metglas 2705M from Metglas [47].

Maximum permeability μ_i	Coercive force A/m	Saturation flux density Tesla	Curie temperature ℃
600,000	1.1	0.77	0.12

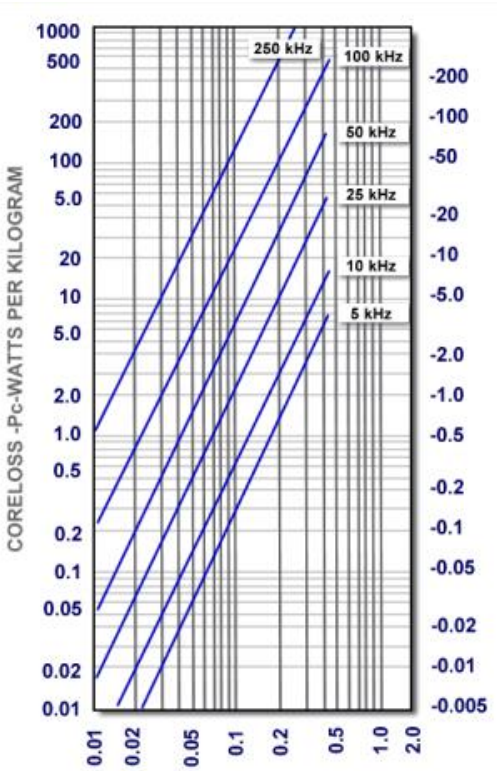

Fig. 26. Core loss density of Metglas 2705M flakes from Metglas [47].

The properties of other materials are the same as aforementioned. Furthermore, each of the setup steps associated with the modeling phase are the same as described in Chapter 3. For this calculation, however, the mesh will be a huge number because the volume is 72 times larger than the model of BCB matrix-permalloy composites. Fortunately, the flakes are in regular cuboid shape, which simplified the mesh generation.

4.3 Simulation results and discussion

The model detailed in the prior section describes a 12.5 wt.% BCB matrix-permalloy-Metglas composite whose relative permeability (as calculated by the ANSYS Maxwell) was shown to be 34 higher than the corresponding BCB matrix-permalloy composite (μ_r=10). When the weight percentage of magnetic particles is 90, the mixture of permalloy and Metglas can generate higher permeability in comparison the permalloy powder only.

Based on simulation results, a 12.5 wt.% BCB matrix-permalloy-Metglas composite material was made in toroid shape and its relative permeability was measured to be 25. In short, the measured result was found to be smaller than the analogous modeled result. This discrepancy could be due to the sedimentation of the Metglas flakes. This phenomenon is much more critical in the BCB matrix-permalloy-Metglas composite material because the mass of each flake is much higher than the permalloy particles. Nonetheless, it must be stressed that 25 is still larger than 10; in other words, the BCB matrix-permalloy-Metglas composite material displayed higher relative permeability in comparison to the the BCB matrix-permalloy composite material.

Moreover, even though adding the flakes can help increase the permeability of the material, the core loss density also increased as well. Fig. 27 shows a comparison between the two materials at 1 MHz (in both calculation estimates and in experimental values). To obtain this graph, we utilized the eddy current mode in Maxwell software, which can calculate core loss density of a given material at different flux density values. Sweep magnetic field strength ranged from 56.5 A/m to 113 A/m, which produced an average B_{ac} from 4 mT to 10 mT.

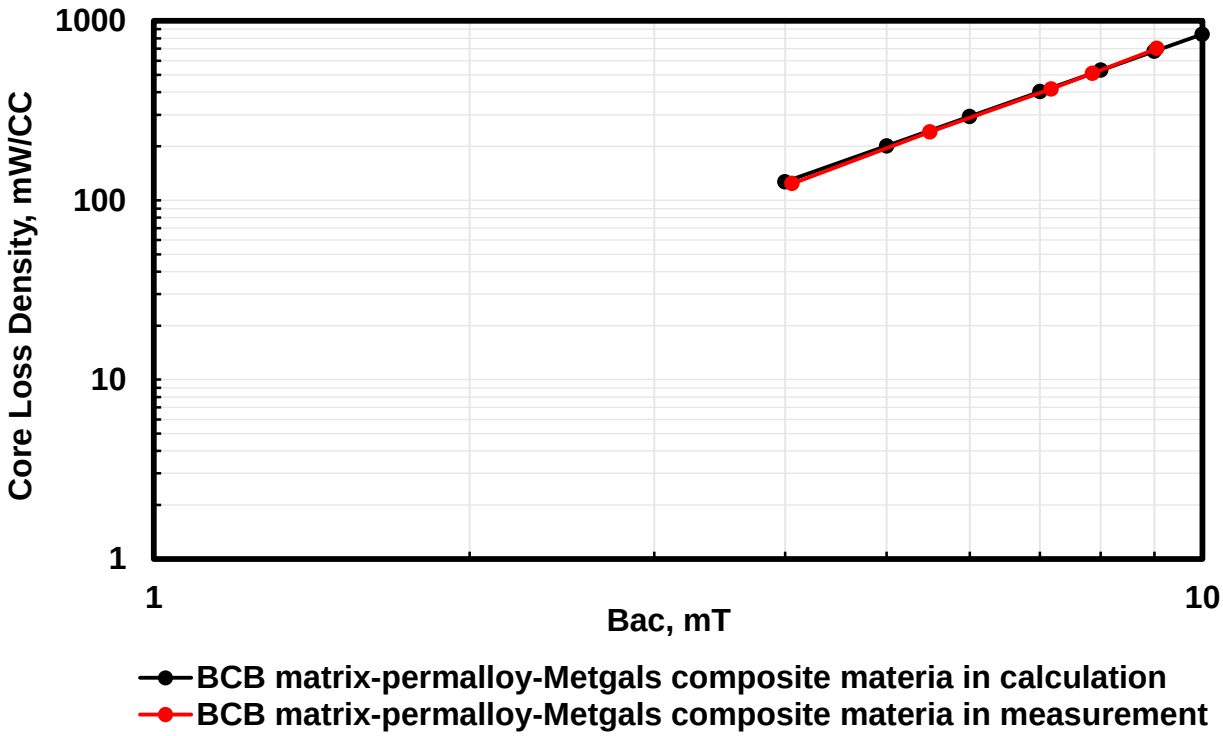

Fig. 27. Comparison of core loss density between BCB matrix-permalloy-Metglas composites and BCB matrix-permalloy composites at 1 MHz.

Both the simulation and the experiment results confirmed that the core loss density of the BCB matrix-permalloy-Metglas composite displayed higher core loss density in comparison to the BCB matrix-permalloy composite. It must be noted that the reason why the measured core loss

density of the BCB matrix-permalloy-Metglas composite agrees with the calculated value is that the core loss in flakes dominates the total core loss of the composite material. Moreover, the model for Metglas flakes is much simpler than the one for permalloy particles. Additionally, since data pertaining to the core loss density of Metglas flakes was obtained from the manufacturer, it is likely to be more accurate.

4.4 Effect of thickness of flakes

Although adding flakes to a composite material can boost its permeability, it can also result in an increase in core loss density. To offset this core loss density effect, two methods are recommended. The first is to decrease the weight percentage of Metglas flakes, and the other involves decreasing the core loss density in each Metglas flake. The second approach will produce a composite with high permeability and low core loss density properties.

Additionally, reducing the thickness of the Metglas flakes can help reduce the core loss density in each flake [48, 49]. Core loss density can be represented via the Steinmetz equation [41],

$$P_v = P_h + P_e \tag{19}$$

where P_v is the total loss in the bulk material; P_h is the hysteresis loss; and P_e is the eddy current loss. At high frequency [48],

$$P_h = \frac{fS\bar{B}_{max}^2 a}{\mu\delta} \tag{20}$$

$$P_e = \frac{\pi^2 f^2 \bar{B}_{max}^2 \sigma a \delta}{2} \tag{21}$$

where f is frequency; S is shape factor; B is flux density; a is the thickness of the flakes; σ is conductivity; δ is skin depth; and μ is permeability.

From the equation (19) to (21), the equation of core loss density is [48]

$$P_v = \frac{fS\bar{B}_{max}^2 a}{\mu\delta} + \frac{\pi^2 f^2 \bar{B}_{max}^2 \sigma a \delta}{2} = \frac{\pi^{\frac{1}{2}} f^{\frac{3}{2}} \bar{B}_{max}^2 \sigma^{\frac{1}{2}} a}{\mu^{\frac{1}{2}}} (\frac{\pi}{2} + S) \quad (22)$$

The equation (22) confirms that the core loss density of a material is linear to its thickness. Therefore, when the thickness of flakes is reduced by half, the core loss density of the flakes is also reduced by half. In other words, to decrease the core loss density of a composite material, decreasing the thickness of flakes represents a valid approach for achieving that goal.

4.4.1 Modeling of different thickness flakes in the model

In order to minimize the variants, the weight or volume percentages of Metglas flakes and permalloy powder are maintained at the same level. The model of our BCB matrix-permalloy-Metglas composite with original thickness of flakes features the magnetic flux in parallel with Metglas flakes—meaning that the flakes are in parallel with flux in the model. So at other thicknesses, the directions of flakes remain the same as the previous one, which is in parallel with the magnetic flux. Fig. 28 depicts a model of different thickness flakes in the composite material. The space inside the copper winding and outside the flakes is filled with a mixture of polymer and permalloy powder, which is not shown.

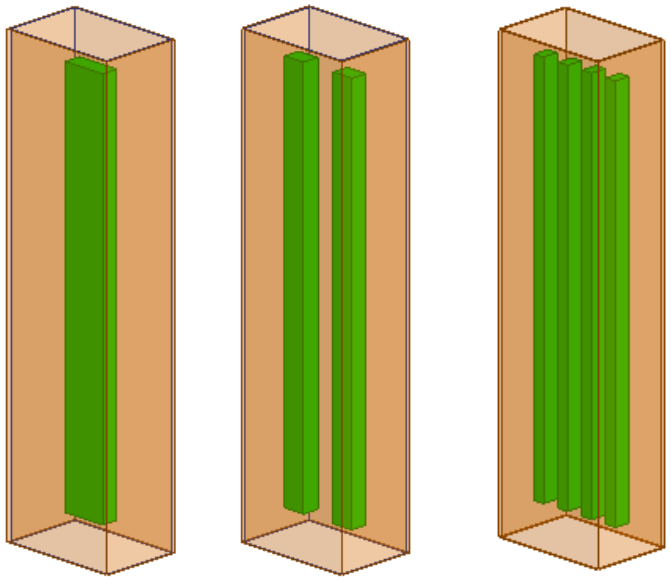

(a) (b) (c)

Fig. 28. Different thickness of flakes in the composite. Orange layer is copper winding and the empty area is the polymer and permalloy mixture. (a) original thickness of flakes (21.3µm), (b) half thickness of flakes (10.65µm), (c) quarter thickness of flakes (5.32µm).

For this simulation, all the calculations setups remained the same as previously described—with the exception of the core loss density data for the flakes. The half thickness Metglas flakes have half core loss density compared to the original thickness ones—and so on to quarter thickness Metglas flakes. Furthermore, a decrease in the size of the flakes with cause the level of mesh to increase, which will slow the speed of calculation.

4.4.2 Thickness of flakes effects on relative permeability of composites

Fig. 29 shows the calculated results of the relative permeability effect of the thickness of Metglas flakes. When the thickness of each Metglas flake is reduced to a quarter of the original thickness, the relative permeability of the composite increases to 14.7 percent. The reason for this outcome

is that when the flakes become thinner, there will be more pieces uniformly distributed in the composite, which decreases the reluctance in the composite. Nonetheless, this percentage is relatively small and can be ignored in future assays. In conclusion, the thickness of flakes does not impact the permeability of the composite.

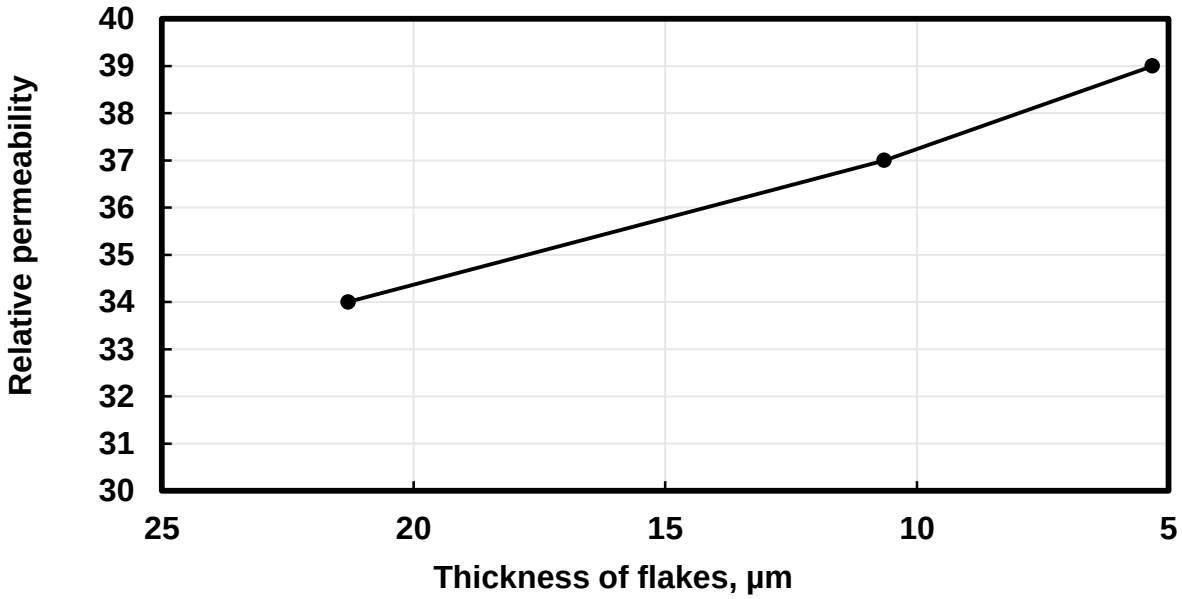

Fig. 29. The relationship between the relative permeability of the BCB matrix-permalloy-Metglas composite and the thickness of the Metglas flakes in the composite.

In contrast, we can state that permeability is impacted by flake distribution—with more uniform distribution of flakes resulting in increased permeability. This relationship is due to the fact that since flakes have less reluctance, more flux will go to the flakes, thereby enhancing permeability (flux distribution is shown in TABLE 8). When the flakes become thinner, the flux distribution will be more uniform, resulting in increased permeability approaching Metglas permeability—but will not reach it. However, because of calculation limitations—with composites featuring

thinner flakes significantly more challenging to model—flakes of one-quarter of original thickness were the thinnest we were able to simulate in our model.

TABLE 8. Flux distribution in BCB matrix-permalloy-Metglas composite with difference thickness of flakes

Thickness of flakes	21.3μm	10.65μm	5.32μm
Flux density in Metglas flakes at the same excitation	0.740mT	0.847mT	0.897mT
Flux density distribution at different composite	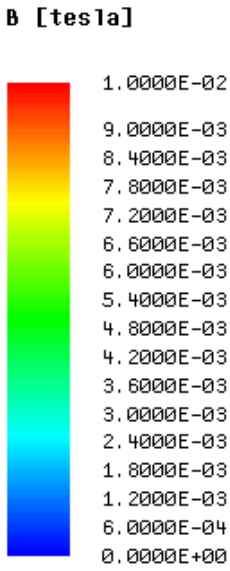	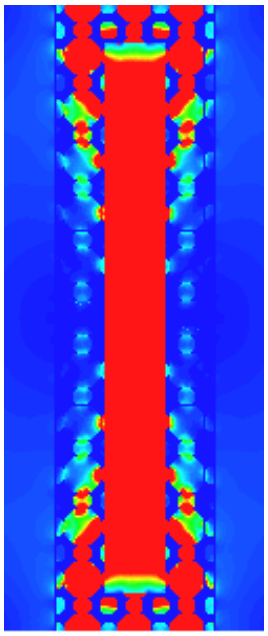	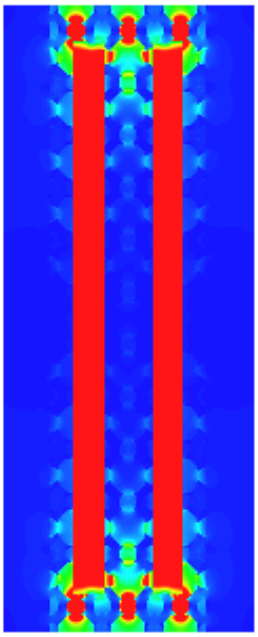	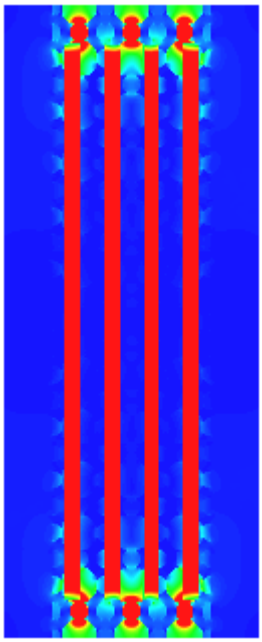

4.4.3 Thickness of flakes effects on core loss density of composites

The main purpose behind decreasing the thickness of Metglas flakes was to decrease the corresponding core loss density of the BCB matrix-permalloy-Metglas composite. This relationship is confirmed by the results depicted in Fig. 30. When the thickness of flakes decreases, the core loss density decreases. Since the reluctance in the flakes is much smaller than

the mixture of permalloy and BCB polymer, almost all the flux goes to the flakes (shown in TABLE 8). Thus, the reduction of loss in the flakes represents the dominant portion of observed total loss. As a result, when the core loss density parameter goes down in flakes, the total core loss of the composite decreases, and the core loss density of the composite decreases as well. Moreover, because the core loss density of Metglas flakes is linear to the thickness of flakes, the loss of the composite is linear to the thickness.

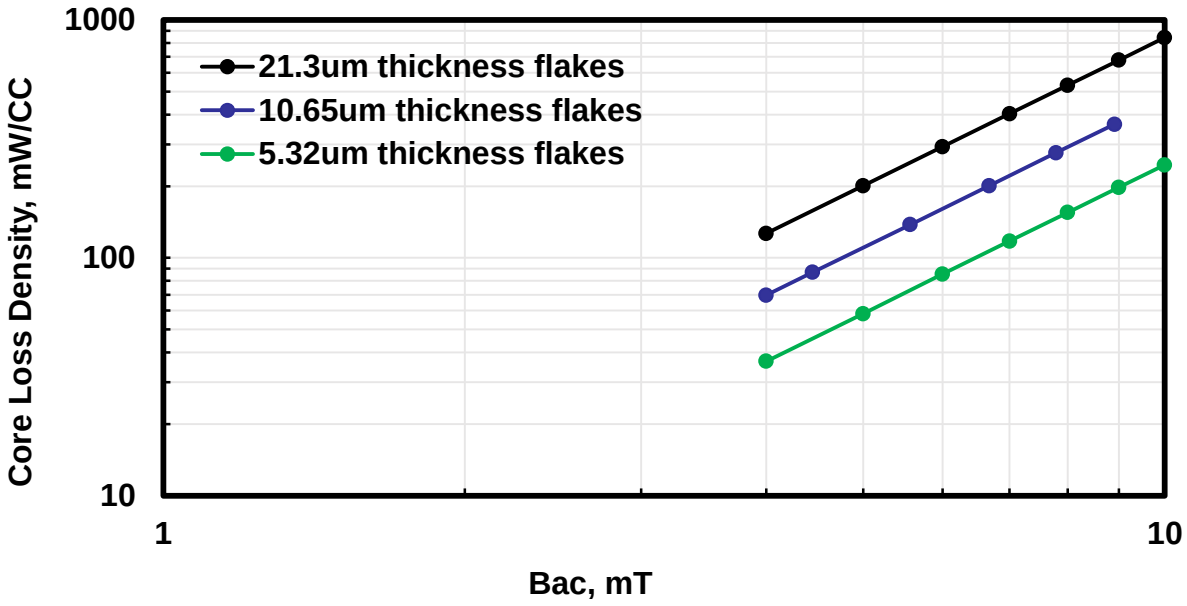

Fig. 30. The relationship between the core loss density at 1 MHz of the BCB matrix-permalloy-Metglas composite and the thickness of the Metglas flakes in the composite

Finally, this model strongly suggests that reducing the thickness of Metglas flakes can help decrease the core loss density of BCB matrix-permalloy-Metglas composite, while at the same time retaining desirable permeability levels.

Chapter 5. Summary and future work

Despite the fact that iron alloys and amorphous alloys feature high permeability, they have low saturation flux density and electrical resistivity. This electrical resistivity introduces high core loss density. Thus, one approach for reducing core loss density is to isolate the magnetic particles. This thesis summarized our investigation of an FE model to analyze the properties of magnetic materials, which could provide guidance for magnetic material formulation.

As described herein, a BCB matrix-permalloy composite was developed whose permeability was been calculated according to an FE model and measured by an impedance analyzer and core loss density setup. To boost the permeability of the BCB matrix-permalloy composite, our model calculations point to the benefit of incorporating Metglas flakes into the composite. While these flakes actually increase permeability levels, they also increase core loss density. Moreover, our simulation results confirm that reducing the thickness of flakes can decrease the core loss density without lowering desired permeability.

In the future, there are three directions that can be taken to further investigate the model. One approach is to develop a simplified model. Indeed, the current model is far too complicated and requires the use of a supercomputer to obtain needed calculations. Additionally, due to the complexity of the model, the tolerance of convergence needs to be higher to obtain desired results. Therefore, the calculated properties have little variation and are not as accurate.

Another avenue for future research lies in conducting more simulations of other magnetic composite materials featuring other formulations or structures. By using different material properties or shapes, it may be possible to synthesize new composite materials with desirable

magnetic properties—for example by rotating the flakes or altering the particle size of the spherical powder.

Finally, the FE model should not only be applied in determining electromagnetic solutions, but also in mechanical analysis. By analyzing the mechanical properties in a more systematic way, the problem of brittle materials at risk for cracking could be minimized.

References

[1] D. M. R. W. Erickson, *Fundamentals of power electronics, 2nd*, 2001.

[2] F. C. Lee, and Qiang Li., *High-Frequency integrated point-of-load converters: Overview.*, 2013.

[3] Y. Su, *High Frequency, High Current 3D Integrated Point-of-Load Module.*, 2015.

[4] Q. Li, *Low-Profile Magnetic Integration for High-Frequency Point-of-Load Converter*, 2011.

[5] B. Estibals, et al., *Design and realisation of integrated inductor with low DC-resistance value for integrated power applications*, 2005.

[6] Y.-J. K. C-H. Ahn, and M-G. Allen,, *Proceedings of 6th International conference on Solid State Sensors and Actuators*, 1993.

[7] C. H. Ahn and M. G. Allen, "Micromachined planar inductors on silicon wafers for MEMS applications," *IEEE Transactions on Industrial Electronics,* vol. 45, pp. 866-876, 1998.

[8] A. W. Lotfi and M. A. Wilkowski, "Issues and advances in high-frequency magnetics for switching power supplies," *Proceedings of the IEEE,* vol. 89, pp. 833-845, 2001.

[9] T. Ge, K. Ngo, and J. Moss, "Point-of-load inductor with high swinging and low loss at light load," in *2016 IEEE Applied Power Electronics Conference and Exposition (APEC)*, 2016, pp. 668-675.

[10] H. Cui, K. D. Ngo, J. Moss, M. H. F. Lim, and E. Rey, "Inductor geometry with improved energy density," *IEEE Transactions on Power Electronics,* vol. 29, pp. 5446-5453, 2014.

[11] D. E. Bogatin, *Looking Under the Sheets: Inductance*, 2007.

[12] A. H. Ball, *Thermal and Electrical Considerations for the Design of Highly-Integrated Point-of-Load Converters*, 2008.

[13] H.-Y. Park, M. J. Schadt, L. Wang, I.-I. S. Lim, P. N. Njoki, S. H. Kim, *et al.*, "Fabrication of magnetic core@ shell Fe oxide@ Au nanoparticles for interfacial bioactivity and bio-separation," *Langmuir,* vol. 23, pp. 9050-9056, 2007.

[14] M. Persson, P. Jansson, A. Jack, and B. Mecrow, "Soft magnetic composite materials-use for electrical machines," in *Electrical Machines and Drives, 1995. Seventh International Conference on (Conf. Publ. No. 412)*, 1995, pp. 242-246.

[15] M. Koledintseva, J. Drewniak, and K. N. Rozanov, *Engineering, modeling and testing of composite absorbing materials for EMC applications*: INTECH Open Access Publisher, 2011.

[16] R. E. Diaz, W. M. Merrill, and N. G. Alexopoulos, "Analytic framework for the modeling of effective media," *Journal of Applied Physics,* vol. 84, pp. 6815-6826, 1998.

[17] J. M. Garnett, "Colours in metal glasses, in metallic films, and in metallic solutions. II," *Philosophical Transactions of the Royal Society of London. Series A, Containing Papers of a Mathematical or Physical Character,* pp. 237-288, 1906.

[18] M. Minelli, M. G. Baschetti, and F. Doghieri, "A comprehensive model for mass transport properties in nanocomposites," *Journal of membrane science,* vol. 381, pp. 10-20, 2011.
[19] V. D. Bruggeman, "Berechnung verschiedener physikalischer Konstanten von heterogenen Substanzen. I. Dielektrizitätskonstanten und Leitfähigkeiten der Mischkörper aus isotropen Substanzen," *Annalen der physik,* vol. 416, pp. 636-664, 1935.
[20] F. de Paulis, M. H. Nisanci, M. Y. Koledintseva, J. L. Drewniak, and A. Orlandi, "From Maxwell Garnett to Debye model for electromagnetic simulation of composite dielectrics Part I: Random spherical inclusions," *IEEE Transactions on Electromagnetic Compatibility,* vol. 53, pp. 933-942, 2011.
[21] H. Shokrollahi and K. Janghorban, "Soft magnetic composite materials (SMCs)," *Journal of Materials Processing Technology,* vol. 189, pp. 1-12, 2007.
[22] R. Pal, "Permeation models for mixed matrix membranes," *Journal of colloid and interface science,* vol. 317, pp. 191-198, 2008.
[23] J. C. Maxwell, *A treatise on electricity and magnetism* vol. 1: Clarendon press, 1881.
[24] L. E. Nielsen, "The thermal and electrical conductivity of two-phase systems," *Industrial & Engineering chemistry fundamentals,* vol. 13, pp. 17-20, 1974.
[25] M. Minelli, F. Doghieri, K. G. Papadokostaki, and J. H. Petropoulos, "A fundamental study of the extent of meaningful application of Maxwell's and Wiener's equations to the permeability of binary composite materials. Part I: A numerical computation approach," *Chemical Engineering Science,* vol. 104, pp. 630-637, 2013.
[26] L. Rayleigh, "LVI. On the influence of obstacles arranged in rectangular order upon the properties of a medium," *The London, Edinburgh, and Dublin Philosophical Magazine and Journal of Science,* vol. 34, pp. 481-502, 1892.
[27] R. E. Meredith and C. W. Tobias, "Resistance to potential flow through a cubical array of spheres," *Journal of applied Physics,* vol. 31, pp. 1270-1273, 1960.
[28] J. Petropoulos, "A comparative study of approaches applied to the permeability of binary composite polymeric materials," *Journal of Polymer Science: Polymer Physics Edition,* vol. 23, pp. 1309-1324, 1985.
[29] Y. Yan, K. D. Ngo, Y. Mei, and G.-Q. Lu, "Additive manufacturing of magnetic components for power electronics integration," in *Electronics Packaging (ICEP), 2016 International Conference on*, 2016, pp. 368-371.
[30] A. Schoppa, P. Delarbre, E. Holzmann, and M. Sigl, "Magnetic properties of soft magnetic powder composites at higher frequencies in comparison with electrical steels," in *IEEE EDPC Conf., Nuremberg (Germany)*, 2013, pp. 29-30.
[31] C. Gélinas, F. Chagnon, and S. Pelletier, "Development of an Iron-Resin composite material for soft magnetic applications," *Advances in Powder Metallurgy and Particulate Materials--1996.,* vol. 6, p. 20, 1996.
[32] J. N. Calata, G.-Q. Lu, and K. Ngo, "Soft Magnetic Alloy–Polymer Composite for High-Frequency Power Electronics Application," *Journal of Electronic Materials,* vol. 43, pp. 126-131, 2014.
[33] K. G. Papadokostaki, M. Minelli, F. Doghieri, and J. H. Petropoulos, "A fundamental study of the extent of meaningful application of Maxwell′ s and Wiener′ s equations to

the permeability of binary composite materials. Part II: A useful explicit analytical approach," *Chemical Engineering Science*, vol. 131, pp. 353-359, 2015.
[34] Wikipedia. *Crystal structure*. Available: https://commons.wikimedia.org/w/index.php?curid=3512107
[35] S. A. Hashemifard, A. F. Ismail, and T. Matsuura, "A new theoretical gas permeability model using resistance modeling for mixed matrix membrane systems," *Journal of Membrane Science*, vol. 350, pp. 259-268, 2010.
[36] W. G. Hurley, and Werner H. Wölfle, *Transformers and inductors for power electronics: theory, design and applications*, 2013.
[37] M. K. Kazimierczuk, *High-frequency magnetic components*, 2009.
[38] T. McLyman, *Transformer and inductor design handbook*, 2004.
[39] E. METALS. *Technical date of permalloy 80*. Available: http://www.espimetals.com/index.php/technical-data/175-permalloy-80
[40] B. Zhang, G. Lu, Y. Feng, J. Xiong, and H. Lu, "Electromagnetic and microwave absorption properties of Alnico powder composites," *Journal of Magnetism and Magnetic Materials*, vol. 299, pp. 205-210, 2006.
[41] S. C. Proteus, "On the law of hysteresis," in *IEEE Proceeding*, 1984, pp. 197-221.
[42] Magnetics. (2000, Core Selection for Saturating Transformers.
[43] I. ANSYS. (2010). *Getting Started with Maxwell: A 2D Magnetostatic Solenoid Problem*. Available: https://www.physicsforums.com/.../tutorial-2d-magnetostatic-solenoid-pdf.78651/
[44] L. Agilent Technologies Japan, "Keysight (formerly Agilent) 4294A - Impedance Analyzer."
[45] D. Tec. *Keysight 16454A Testadapter für magnetisches Material bis 1 GHz*. Available: http://www.datatec.de/Keysight-16454A-Testadapter.htm
[46] M. Mu, Q. Li, D. J. Gilham, F. C. Lee, and K. D. Ngo, "New core loss measurement method for high-frequency magnetic materials," *IEEE Transactions on Power Electronics*, vol. 29, pp. 4374-4381, 2014.
[47] Metglas. (2014, Magnetic Alloy 2705M (cobalt-based)
[48] J. Barranger, "Hysteresis and eddy-current losses of a transformer lamination viewed as an application of the pointing theorem [Электронный ресурс]," *J. Barranger.—Washington: NASA Technical note*, 1965.
[49] G. E. Schwarze, W. R. Wieserman, and J. M. Niedra, "Magnetic and Electrical Characteristics of Permalloy Thin Tape Bobbin Cores," in *2nd International Energy Conversion Engineering Conference, Providence, Rhode Island*, 2004, pp. 16-19.